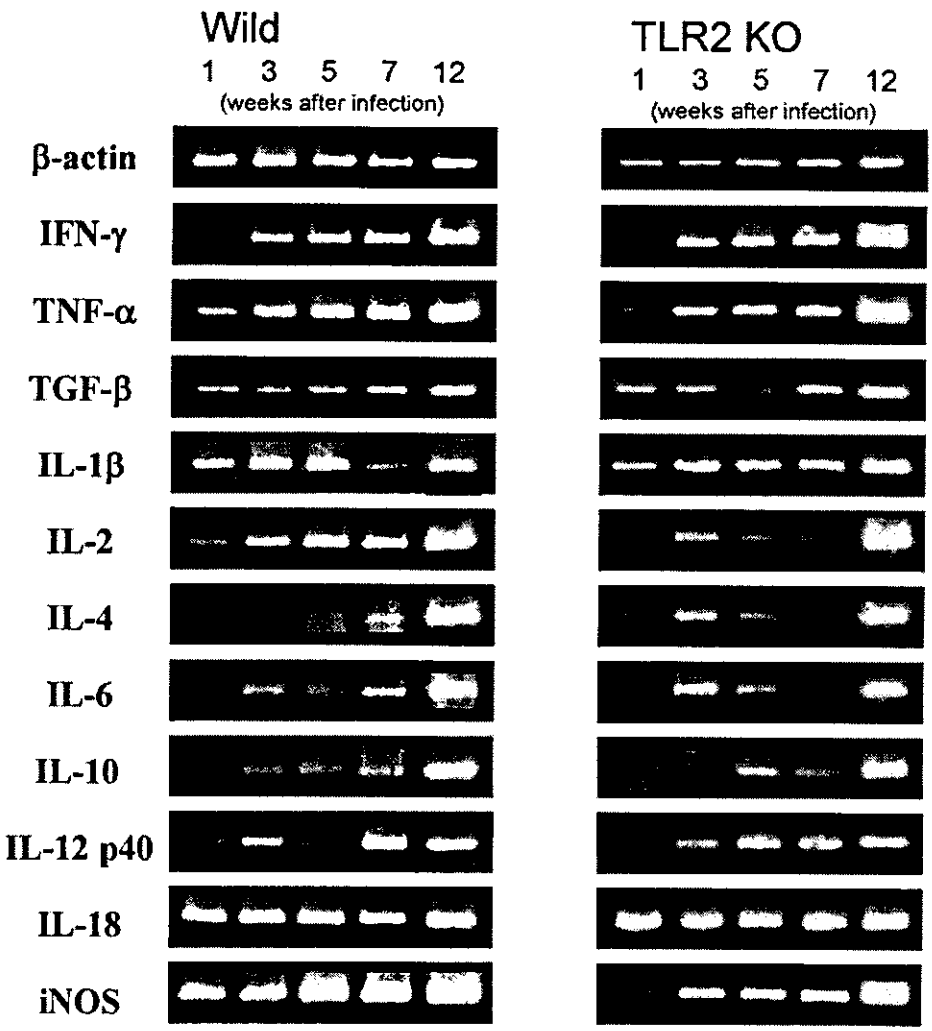

Fig. 5. *In vivo* expression of mRNAs for various cytokines and iNOS in Kurono strain-infected mice by RT-PCR. The lung tissues of TLR2 KO and WT mice (three mice each/time point) were removed 1, 3, 5, 7, and 12 weeks after the airborne infection. β-actin gene primer sets were used as an internal control. TNF-α, IL-2, TGF-β, and iNOS mRNA expression is low in TLR2 KO mice.

subjected to autoradiography for 5 days. As shown in Fig. 6, mycobacterial infection of WT mice for 1 and 5 weeks increased nuclear protein binding to the labeled oligonucleotide DNA of the NF-κB gene, whereas infection of TLR2 KO mice did not do so. The nuclear proteins from infected lung tissues of WT mice bound significantly to the specific oligonucleotide DNA, but those from infected lung tissues of TLR2 KO mice did not do so.

Discussion

We investigated the *in vivo* roles of TLR (TLR2 and TLR6) in mycobacterial infection. In the absence of TLR2, but not TLR6, the TLR2 KO mice were relatively susceptible to *M. tuberculosis* infection, but absence of TLR2 was not lethal to the animal. Under these conditions, TNF-α, TGF-β, IL-1β, IL-2, and iNOS mRNA expression levels were significantly lower, and IFN-γ mRNA expression level was slightly lower, than in wild-type mice. It has been reported that IFN-γ and TNF-α play a major role in defense against mycobacterial infection (8, 11, 12, 15, 21). Low expression of IFN-γ and TNF-α mRNA in the TLR2 KO mice may also explain the more pronounced pulmonary granulomatous lesions.

It is important to examine the roles of various transcription factors in inflammatory processes, because they control the expression of major cytokines. It has been reported that NF-κB and AP-1 are activated through the IL-1 receptor/TLR signaling pathway (3, 30). In our experiments, both NF-κB activities were low in

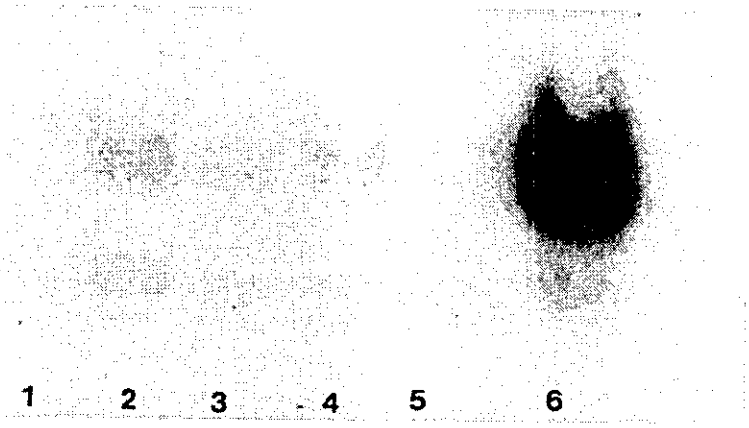

Fig. 6. NF-κB (lanes 1 through 4) activities in lung tissues at 1 and 5 weeks after infection. Lane 1, lung tissues from TLR2 KO mice 1 week after infection; lane 2, lung tissues from WT mice 1 week after infection; lane 3, lung tissues from TLR2 KO mice 5 weeks after infection; lane 4, lung tissues from WT mice 5 weeks after infection; lane 5, competition of the nuclear protein in lung tissues from WT mice 5 weeks after infection with the unlabeled oligonucleotides and lane 6, lung tissues from WT mice treated with 2 μg LPS intratracheally. NF-κB activities are low in infected TLR2 KO mice compared with those of WT mice.

TLR2 KO mice. Under these conditions, the expression of IL-1β, IL-2, and TNF-α mRNA, which are regulated by NF-κB, was low. The reason why TLR2 deficiency in mycobacterial infection is not lethal is that there is another mechanism of NF-κB activation via IL-1 and TNF-α.

iNOS mRNA expression was also depressed in TLR2 KP mice. As evaluated by electron microscopy, tubercle bacilli were replicating in epithelioid macrophage phagosomes. In fact, the NO activity of alveolar macrophages from TLR2 KO mice was significantly lower than that from WT mice as assessed by an NO assay with Griess reagent (data not shown). Low NO activity is a result of reduced iNOS mRNA expression in the absence of TLR2.

It has been reported that TLR2 alone mediates mycobacteria-induced proinflammatory signaling in macrophages (28) and that activation of TLR2 leads to killing of intracellular *M. tuberculosis* in both mouse and human macrophages (27). Bulut et al. have shown that TLR2 and TLR6 cooperate in cellular activation by soluble tuberculosis factor and *Borrelia burgdorferi* outer surface protein A lipoprotein (7). A soluble heat-stable and protease-resistant mycobacterial factor mediates TLR2-dependent activation, whereas a heat-sensitive cell-associated mycobacterial factor mediates TLR4-dependent activation (17). It is controversial whether cellular activation by *M. tuberculosis* is mediated by TLR2 alone or by TLR2 with the cooperation of TLR4 or TLR6. Our *in vivo* study indicates strongly that TLR2 does not play an essential role in defense against mycobacterial infection. However, this does not rule out the possibility that TLR2 cooperates with TLR4 in protection against mycobacterial infection because TLR4 expression is required to control chronic *M. tuberculosis* infection in mice (1). There was no significant difference between TLR6 KO and WT mice infected with *M. tuberculosis* in pulmonary granuloma size and bacterial load of infected lung and spleen tissues.

Expression levels of IL-4 and IL-6 mRNA are high in TLR2 KO mice. IL-4 and IL-6 play a role in defence against mycobacterial infection (16, 22). In the absence of IL-4, mice develop pulmonary granulomas that are larger than those in WT mice (22), and lethal tuberculosis develops in IL-6-deficient mutant mice (16). Our data clearly show that high expression of IL-4 and IL-6 mRNA results in granulomatous pulmonary lesions lacking central necrosis, not multifocal necrotic lung lesions.

TGF-β mRNA was depressed in our *M. tuberculosis*-infected TLR2 KO mice, whereas TGF-β mRNA was expressed normally in NF-κB p50 KO mice (30). TGF-β was localized to mononuclear phagocytes of tuberculous lung lesions in 4 (33%) of 12 tuberculosis patients (5). TGF-β can be induced in human monocytes by the lipoarabinomannan of *M. tuberculosis* (9). TGF-β, although it is not universally expressed, may be involved in the development and/or consequences of tuberculous granuloma formation. Further study will be required to clarify the role of TGF-β in mycobacterial infection, because TGF-β mRNA expression was low in the TLR2 KO mice.

In summary, TLR2 is important for the interaction of host cells with mycobacteria that results in activation of NF-κB, and this interaction plays a significant role in defense against mycobacterial infection.

This study was supported in part by an International Collaborative Study Grant to the chief investigator, Dr. Isamu Sugawara, from the Ministry of Health, Labour and Welfare, Japan. We would like to acknowledge the help of Dr. Masashi Desaki, University of Tokyo Faculty of Medicine, with the electrophoresis mobility shift assay (EMSA) for NF-κB.

References

1) Abel, B., Thieblemont, N., Quesniaux, V.J.F., Brown, N., Mpagi, J., Miyake, K., Bihl, F., and Ryffel, B. 2002. Toll-like receptor 4 expression is required to control chronic *Mycobacterium tuberculosis* infection in mice. J. Immunol. **169**: 3155–3162.
2) Aderem, A., and Ulevitch, R.J. 2000. Toll-like receptors in the induction of the innate immune response. Nature **406**: 782–787.
3) Akira, S., Takeda, K., and Kaisho, T. 2001. Toll-like receptors: critical proteins linking innate and acquired immunity. Nature Immunol. **2**: 675–680.
4) Anderson, K.V. 2000. Toll signaling pathways in the immune response. Curr. Opin. Immunol. **12**: 13–19.
5) Aung, H., Toossi, Z., McKenna, S.M., Gogate, P., Sierra, J., Sada, E., and Rich, E.A. 2000. Expression of transforming growth factor-β but not tumor necrosis factor-α, interferon-γ, and interleukin-4 in granulomatous lung lesions in tuberculosis. Tuber. Lung Dis. **80**: 61–67.
6) Brightbill, H.D., Libraty, D.M., Krutzik, S.R., Yang, R.B., Belisle, J.T., Bleharski, J.R., Maitland, M., Norgard, M.V., Plevy, S.E., Smale, S.T., Brennan, P.J., Bloom, B.R., Godowski, P.J., and Modlin, R.L. 1999. Host defense mechanisms triggered by microbial lipoproteins through the TLR receptors. Science **285**: 732–736.
7) Bulut, Y., Faure, E., Thomas, L., Equils, O., and Arditi, M. 2001. Cooperation of Toll-like receptor 2 and 6 for cellular activation by soluble tuberculosis factor and *Borrelia burgdorferi* outer surface protein A lipoprotein: role of Toll-interacting protein and IL-1 receptor signaling molecules in Toll-like receptor 2 signaling. J. Immunol. **167**: 987–994.
8) Cooper, A.M., Dalton, D.K., Stewart, T.A., Griffin, J.P., Douglas, D.G., and Orme, I.M. 1993. Disseminated tuberculosis in interferon-γ gene-disrupted mice. J. Exp. Med. **178**: 2243–2247.
9) Dahl, K.E., Shiratuchi, H., Hamilton, B.D., Ellner, J.J., and Toossi, Z. 1996. Selective induction of transforming growth factor β in human monocytes by lipoarabinomannan of *Mycobacterium tuberculosis*. Infect. Immun. **64**: 399–405.
10) Deryckere, F., and Cannon, F. 1994. A one-hour minipreparation technique for extraction of DNA-binding proteins from animal tissues. Biotechniques **16**: 405.
11) Flynn, J.L., Chan, J.J., Triebold, K.J., Dalton, D.K., Stewart, T.A., and Bloom, B.R. 1993. An essential role for interferon-γ in resistance to *Mycobacterium tuberculosis* infection. J. Exp. Med. **178**: 2249–2254.
12) Flynn, J.L., Goldstein, M.M., Chan, J., Triebold, K.J., Pfeffer, K., Lowenstein, C.J., Schreiber, R., Mak, T.W., and Bloom, B.R. 1995. Tumor necrosis factor-α is required in the protective immune response against *Mycobacterium tuberculosis* in mice. Immunity **2**: 561–572.
13) Hayashi, F., Smith, K.D., Ozinsky, A., Hawn, T.R., Yi, E.C., Goodlett, D.R., Eng, J.K., Akira, S., Underhill, D.M., and Aderem, A. 2001. The innate immune response to bacterial flagellin is mediated by Toll-like receptor 5. Nature **410**: 1099–1103.
14) Henmi, H., Takeuchi, O., Kawai, T., Kaisho, T., Sato, S., Sanjo, H., Matsumoto, M., Hoshino, K., Wagner, H., Takeda, K., and Akira, S. 2001. A Toll-like receptor recognizes bacterial DNA. Nature **408**: 740–745.
15) Kaneko, H., Yamada, H., Kazumi, Y., Mizuno, S., Sekikawa, K., and Sugawara, I. 1999. Role of tumor necrosis factor-α in *Mycobacterium*-induced granuloma formation in tumor necrosis factor-α-deficient mice. Lab. Invest. **79**: 379–386.
16) Ladel, C.H., Blum, C., Dreher, A., Reifenberg, K., Kopf, M., and Kaufmann, S.H. 1997. Lethal tuberculosis in interleukin-6-deficient mutant mice. Infect. Immun. **65**: 4843–4849.
17) Means, T.K., Wang, S., Lien, E., Yoshimura, A., Golenbock, D.T., and Fenton, M.J. 1999. Human Toll-like receptors mediate cellular activation by *Mycobacterium tuberculosis*. J. Immunol. **163**: 3920–3927.
18) Means, T.K., Jones, B.W., Schromm, A.B., Shurtleff, B.A., Smith, J.A., Keane, J., Golenbock, D.T., Vogel, S.N., and Fenton, M.J. 2001. Differential effects of a Toll-like receptor antagonist on *Mycobacterium tuberculosis*-induced macrophage responses. J. Immunol. **166**: 4074–4082.
19) Nishiguchi, M., Matsumoto, M., Takao, T., Hoshino, M., Shimonishi, Y., Tsuji, S., Begum, N.A., Takeuchi, O., Akira, S., Toyoshima, K., and Seya, T. 2001. *Mycoplasma fermentans* lipoprotein M161 Ag-induced cell activation is mediated by Toll-like receptor 2: role of N-terminal hydrophobic portion in its multiple functions. J. Immunol. **166**: 2610–2616.
20) Noss, E.H., Pai, R.K., Sellati, T.J., Radolf, J.D., Belisle, J., Golenbock, D.T., Boom, W.H., and Harding, C.V. 2001. Toll-like receptor 2-dependent inhibition of macrophage class II MHC expression and antigen processing by 19-kDa lipoprotein of *Mycobacterium tuberculosis*. J. Immunol. **167**: 910–918.
21) Sugawara, I., Yamada, H., Ohtomo, K., Aoki, T., Doi, N., Kazumi, Y., Tagawa, Y., and Iwakura, Y. 1998. Granulomas in IFN-γ gene-disrupted mice are inducible by avirulent *Mycobacterium*, but not by virulent *Mycobacterium*. J. Med. Microbiol. **47**: 871–877.
22) Sugawara, I., Yamada, H., Mizuno, S., and Iwakura, Y. 2000. IL-4 is required for defense against mycobacterial infection. Microbiol. Immunol. **44**: 971–979.
23) Sugawara, I., Mizuno, S., Yamada, H., Matsumoto, M., and Akira, S. 2001. Disruption of nuclear factor-interleukin-6, a transcription factor, results in severe mycobacterial infection. Am. J. Pathol. **158**: 361–366.
24) Sugawara, I., Yamada, H., Mizuno, S., Li, C., Nakayama, T., and Taniguchi, M. 2002. Mycobacterial infection in natural killer T cell knockout mice. Tuberculosis **82**: 97–104.
25) Takeuchi, O., Hoshino, K., Kawai, T., Sanjo, H., Takada, H., Ogawa, T., Takeda, K., and Akira, S. 1999. Differential roles of TLR2 and TLR4 in recognition of Gram-negative and Gram-positive bacterial cell wall components. Immuni-

ty **11**: 443–451.

26) Takizawa, H., Ohtoshi, T., Kawasaki, S., Kohyama, T., Desaki, M., Kasama, T., Kobayashi, K., Nakahara, K., Yamamoto, K., Matsushima, K., and Kudoh, S. 1999. Diesel exhaust particles induce NF-κB activation in human bronchial epithelial cells *in vitro*: importance in cytokine transcription. J. Immunol. **162**: 4705–4711.

27) Thoma-Uszynski, S., Stenger, S., Takeuchi, O., Ochoa, M.T., Engele, M., Sieling, P.A., Barnes, P.F., Rollinghoff, M., Bolcskei, P.L., Wagner, M., Akira, S., Norgard, M.V., Belisle, J.T., Godowski, P.J., Bloom, B.R., and Modlin, R.L. 2000. Induction of direct antimicrobial activity through mammalian Toll-like receptors. Science **291**: 1544–1547.

28) Underhill, D.M., Ozinsky, A., Smith, K.D., and Aderem, A. 1999. Toll-like receptor-2 mediates mycobacteria-induced proinflammatory signaling in macrophages. Proc. Natl. Acad. Sci. U.S.A. **96**: 14459–14463.

29) Yamada, H., Mizuno, S., Horai, R., Iwakura, Y., and Sugawara, I. 2000. Protective role of interleukin-1 in mycobacterial infection in IL-1 α/β double-knockout mice. Lab. Invest. **80**: 759–767.

30) Yamada, H., Mizuno, S., Reza-Gholizadeh, M., and Sugawara, I. 2001. Relative importance of NF-κB p50 in mycobacterial infection. Infect. Immun. **69**: 7100–7105.

Journal of Medical Microbiology (2003), 52, 29–34 DOI 10.1099/jmm.0.05026-0

Relative importance of STAT4 in murine tuberculosis

I. Sugawara, H. Yamada and S. Mizuno

Correspondence
I. Sugawara
sugawara@jata.or.jp

Department of Molecular Pathology, The Research Institute of Tuberculosis, Japan Anti-Tuberculosis Association, 3-1-24 Matsuyama, Kiyose, Tokyo 204-0022, Japan

Received 11 July 2002
Accepted 13 September 2002

This study was designed to determine the roles of STAT proteins in defence against mycobacterial infection. Airborne infection of STAT4 knockout (KO) mice with a *Mycobacterium tuberculosis* strain induced large granulomas with massive neutrophil infiltration over time, while that in STAT6 KO mice did not. The STAT4 KO mice succumbed to mycobacterial infection by the 80th day after infection. Compared with the levels in wild-type (WT) and STAT6 KO mice, pulmonary inducible nitric oxide synthase, interferon-α, -β and -γ mRNA levels were significantly lower in STAT4 KO mice, but expression of interleukin-2, -6, -12 and -18 mRNAs was slightly higher up to the fifth week after aerial infection. Therefore, STAT4, but not STAT6, appears to be a critical transcription factor in mycobacterial regulation.

INTRODUCTION

Interferon (IFN)-stimulated gene factor 3 is a heterotrimeric transcription factor that consists of p48, p91 and p113. p91 was named 'signal transducer and activator of transcription' (STAT) 1 and p113 has been named STAT3 (Darnell, 1997). Other STAT proteins have since been found, and the STAT family consists of seven transcription factors. Among them, STAT4 is activated in response to stimulation with interleukin (IL)-12. In STAT4 knockout (KO) mice, Th1-helper T-cell development is inhibited and lymphocytic proliferation in response to IL-12, induction of IFN-γ expression and activation of natural killer (NK) cells are abrogated (Kaplan *et al.*, 1998). It is thought that the STAT4 and STAT6 proliferation signals are regulated via inhibition of induction of $p27^{Kip1}$ (Kaplan *et al.*, 1998). However, STAT6 is activated after stimulation with IL-4. In STAT6 KO mice, the disappearance of Th2 lymphocytes and proliferative abrogation of lymphocytes by IL-4 have been reported (Darnell, 1997).

Tuberculosis is a chronic, airborne infectious disease. It has been reported that IFN-γ, a Th1 cytokine, and tumour necrosis factor (TNF)-α, IL-12 and IL-18, which affect Th1 T-cell development, are implicated in the pathogenesis of mycobacterial infection (Flynn *et al.*, 1993, 1995; Cooper *et al.*, 1993, 1997; Sugawara *et al.*, 1998, 1999; Kindler *et al.*, 1989; Kaneko *et al.*, 1999). We are interested in the roles of transcription factors that regulate cytokine expression in mycobacterial infection. We found that the transcription factor nuclear factor (NF)-IL-6 is critical in mycobacterial control as well as in the induction of the granulocyte-colony-stimulating factor in alveolar macrophages that results in neutrophil activation (Sugawara *et al.*, 2001). We have also reported that NF-κB p50 KO mice develop multifocal necrotic pulmonary lesions or lobar pneumonia and that the interaction of NK-κB with host cells plays an important role in the pathogenesis of tuberculosis (Yamada *et al.*, 2001). These findings, together with reports on roles of STAT4 and STAT6 proteins in lymphocyte development, prompted us to explore the roles of STAT proteins in mycobacterial infection. We report here that STAT4, but not STAT6, plays an important role in defence against mycobacterial infection.

Abbreviations: IFN, interferon; IL, interleukin; iNOS, inducible nitric oxide synthase; KO, knockout; TGF, transforming growth factor; TNF, tumour necrosis factor.

METHODS

Animals. Six-week-old BALB/c wild-type (WT) mice were purchased from Japan SLC Co. Ltd and BALB/c STAT4 KO and STAT6 KO mice (Kaplan *et al.*, 1996a, b) were purchased from Jackson Laboratories (20 mice per group). The KO mice showed no developmental abnormalities. All mice were housed in a biosafety level 3 facility and were given mouse chow and water *ad libitum* after aerosol infection with virulent mycobacteria.

Experimental infections. The virulent Kurono strain of *Mycobacterium tuberculosis* (ATCC 35812) was grown in Middlebrook 7H9 broth for 2 weeks and then filtered using a sterile acrodisc syringe filter (Pall Corp.) with a pore size of 5·0 μm. Aliquots of the bacterial solution were stored at −80 °C until use. The mice were infected via the airborne route by placing them into the exposure chamber of a Glas-Col aerosol generator. The nebulizer compartment was filled with 5 ml of a suspension containing 10^6 c.f.u. of Kurono tubercle bacilli so that approximately 100 bacteria would be deposited in the lungs of each animal (Sugawara *et al.*, 1999; Yamada *et al.*, 2001). Several infected mice were followed up to 80 days for survival.

Titration of mycobacteria (c.f.u. assay). At 1, 3, 5 and 7 weeks after aerial infection, mice were anaesthetized with pentobarbital sodium, the abdominal cavity was opened and the mice were exsanguinated after splenectomy. Lungs, spleens and livers were excised and weighed. The

left lobe of each lung and a part of the spleen tissue were weighed separately and used to evaluate *in vivo* growth of mycobacteria. The lung and spleen tissues were homogenized with a mortar and pestle and 1 ml sterile saline was added. Next, 100 µl homogenate was plated in a 10-fold serial dilution on 1 % (v/v) Ogawa's egg medium. Colonies on the medium were counted after a 4-week incubation at 37 °C (Yamada *et al.*, 2001).

RT-PCR. Parts of the right lobe of the lung and the spleen tissue that remained after the c.f.u. assay were used to perform RT-PCR analysis for mRNA expression of several cytokines and inducible nitric oxide synthase (iNOS) during infection. These tissue samples were snap-frozen in liquid nitrogen and stored at −85 °C until use. RNA extraction was performed as described previously (Sugawara *et al.*, 2001; Yamada *et al.*, 2001). Briefly, frozen tissues were homogenized using a microcentrifuge tube and a tip-closed 1 ml pipette in liquid nitrogen. The homogenates were treated with the total RNA isolation reagent TRIzol (Gibco-BRL) according to the manufacturer's instructions. After RNA isolation, the total RNA concentration was measured and the RNA was then reverse-transcribed into cDNA with M-MLV reverse transcriptase (Gibco-BRL) and agarose gel electrophoresis was performed.

The PCR was performed with gene-specific primer sets for β-actin, IFN-α, -β and -γ, TNF-α, IL-1β, -2, -4, -6, -10, -12p40 and IL-18, transforming growth factor (TGF)-β and iNOS. The DNA sequences of the primer sets and corresponding PCR conditions are summarized in Table 1. Amplification was carried out with a DNA thermal cycler 480 (Perkin-Elmer Cetus). The PCR product (10 µl) was applied for electrophoresis on a 4 % (w/v) agarose and NuSieve GTG (1:3) gel and visualized using ethidium bromide staining. Thereafter, we conducted a densitometric analysis of the electrophoretic RT-PCR results using the NIH Image software version 1.62. Relative densitometric ratios were determined with β-actin mRNA as an internal control (Sugawara *et al.*, 2002).

Light and electron microscopic examination. For light microscopic examination, the right middle lobe of each lung was excised and fixed with a 20 % (v/v) formalin buffered methanol solution, Mildform 20 NM [containing 8 % (v/v) formaldehyde and 20 % (v/v) methanol, Wako Pure Chemical Co.], dehydrated with a graded series of ethanol, treated with xylene and embedded in paraffin. Sections 5-mm-thick were cut from each paraffin block and stained with either haematoxylin and eosin or Ziehl–Neelsen stains.

For electron microscopy, the right lower lobe of each lung was fixed with 2·5 % (w/v) glutaraldehyde in 0·1 M phosphate buffer (pH 7·4) at 4 °C overnight, washed three times with cold phosphate buffer, post-fixed with 1 % (w/v) osmium tetroxide in phosphate buffer at 4 °C for 1 h, dehydrated with a graded series of ethanol containing 10 % (v/v) methanol and finally embedded in Spurr's low-viscosity resin. Ultrathin sections were cut using a Reichert Ultracut ultramicrotome and stained with uranyl acetate and Sato's lead solution. Stained ultrathin sections were examined with a JEOL JEM-1230 electron microscope (Yamada *et al.*, 2001).

Table 1. PCR primer sets used in this study

Target	Sequence	Annealing temperature (°C)	Cycles (*n*)	Product length (bp)
β-actin	Sense: 5′-TGTGATGGTGGGAATGGGTCAG-3′ Antisense: 5′-TTTGATGTCACGCACGATTTCC-3′	65	23	514
IFN-α	Sense: 5′-ATGGCTAGGCTCTGTGCTTTCCT-3′ Antisense: 5′-AGGGCTCTCCAGAYTTCTGCTCTG-3′	68	30	524
IFN-β	Sense: 5′-CATCAACTATAAGCAGCTCCA-3′ Antisense: 5′-TTCAAGTGGAGAGCAGTTGAG-3′	65	33	354
IFN-γ	Sense: 5′-TACTGCCACGGCACAGTCATTGAA-3′ Antisense: 5′TAGGCGACTCCTTTTCCGCTTCCT-3′	65	30	405
TNF-α	Sense: 5′-ATGAGCACAGAAAGCATGATC-3′ Antisense: 5′-TACAGGCTTGTCACTCGAATT-3′	65	30	276
IL-1β	Sense: 5′-CAGGATGAGGACATGAGCACC-3′ Antisense: 5′-CTCTGCAGACTCAAACTCCAC-3′	65	30	447
IL-2	Sense: 5′-CTTCAAGCTCCACTTCAAGCT-3′ Antisense: 5′-CCATCTCCTCAGAAAGTCCAC-3′	65	40	400
IL-4	Sense: 5′-ACGGAGATGGATGTGCCAAACGTC-3′ Antisense: 5′-CGAGTAATCCATTTGCATGATGC-3′	65	40	279
IL-6	Sense: 5′-CATCCAGTTGCCTTCTTGGGA-3′ Antisense: 5′-CATTGGGAAATTGGGGTAGGAAG-3′	65	40	463
IL-10	Sense: 5′-GTGAAGACTTTCTTTCAAACAAAG-3′ Antisense: 5′-CTGCTCCACTGCCTTGCTCTTATT-3′	56	40	273
IL-12p40	Sense: 5′-ATCTCCTGGTTTGCCATCGTTTTG-3′ Antisense: 5′-TCCCTTTGGTCCAGTGTGACCTTC-3′	65	30	527
IL-18	Sense: 5′-ACTGTACAACCGCAGTAATACGG-3′ Antisense: 5′-TCCATCTTGTTGTGTCCTGG-3′	58	35	319
TGF-β	Sense: 5′-CGGGGCGACCTGGGCACCATCCATGAC-3′ Antisense: 5′-CTGCTCCACCTTGGGCTTGCGACCCAC-3′	65	24	405
iNOS	Sense: 5′-TGGGAATGGAGACTGTCCCAG-3′ Antisense: 5′-GGGATCTGAATGTGATGTTTG-3′	65	30	306

Statistical methods. Values were compared using Student's *t* test. For all statistical analyses, a value of $P < 0.01$ was considered significant.

RESULTS

Mycobacterial burden in the lungs and spleens of STAT KO mice

STAT4 KO mice died of disseminated tuberculosis by the 80th day after aerosol infection, whereas WT and STAT6 KO mice survived until the day they were killed (data not shown). Up until 3 weeks after aerial infection, there were no significant differences in lung and spleen titres between STAT4 KO mice and BALB/c WT mice; both groups possessed similar titres, approximately 10^5 c.f.u. in the lungs. However, after 9 weeks post-infection, many STAT4 KO mice succumbed to the mycobacterial infection. Mycobacterial titres in the lung and spleen tissues exceeded 10^6 c.f.u. At this time-point, there were statistically significant differences in both lung and spleen counts between WT and STAT4 KO mice ($P < 0.01$) (Fig. 1a). There were no statistically significant differences in lung and spleen counts between STAT6 KO and WT mice ($P < 0.01$) (Fig. 1b).

Light and electron microscopic observations of infected lungs

Consistent with the changes in mycobacterial burden, the histopathological findings from STAT4 KO and WT mice showed similar changes at 5 weeks after infection, but at 9 weeks, STAT4 KO mice showed multifocal necrotic lesions in the lung, liver and spleen. Each necrotic lesion was characterized by central necrosis, with massive accumulation of tubercle bacilli. These severe histopathological changes were not observed in the WT or STAT6 KO mice.

Electron microscopy demonstrated that alveolar macrophages in STAT4 KO mice phagocytosed more tubercle bacilli and that the engulfed tubercle bacilli were located in phagosomes and appeared to escape the killing mechanisms of the host cells. No escape of *M. tuberculosis* from phagosomes to cytoplasm was observed. The tubercle bacilli in the phagosomes of epithelioid macrophages were relatively long and contained many large vacuole-like structures (Fig. 2).

RT-PCR analysis

Fig. 3 shows the results of densitometric analysis of the RT-PCR data from infected lung tissues. In STAT4 KO mice, expression of IFN-α, IFN-β, IFN-γ and iNOS mRNA was low at weeks 1–5 after infection compared with that of WT mice. Expression of TNF-α, IL-1β, IL-4, IL-10 and IL-12 mRNA was similar in STAT4 KO mice and WT mice. However, IL-2, IL-6, IL-18 and TGF-β mRNA were expressed at slightly higher levels in STAT4 KO mice than in WT mice. No significant differences were found between STAT6 KO and WT mice in expression of cytokine, TGF-β or iNOS mRNAs (data not shown).

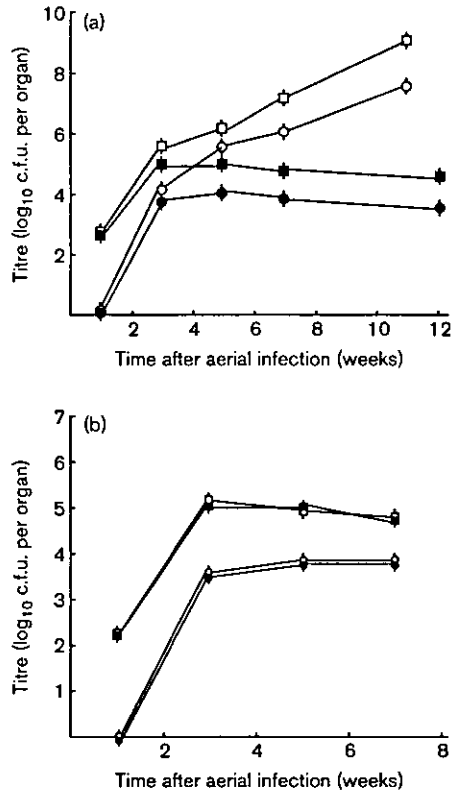

Fig. 1. Mycobacterial titres in lungs (□) and spleens (○) of STAT4 KO (a) and STAT6 KO (b) mice exposed to 10^6 c.f.u. *M. tuberculosis* Kurono strain by the airborne route. Lungs (■) and spleens (●) of WT mice were included in each experiment. At the indicated times after infection, four mice from each group were killed and homogenates of lung and spleen tissues were plated on 7H10 agar. Error bars indicate SEM.

DISCUSSION

The purpose of our study was to determine the roles of STAT proteins as transcription factors in the pathogenesis of murine tuberculosis. We have shown that STAT4, but not STAT6, is essential for the control and survival of the *M. tuberculosis* infection. At the same time, the levels of IFN-α, IFN-β, IFN-γ and iNOS mRNA expression were low until the fifth week after infection in STAT4 KO mice. We repeated the experiments twice and the results thus obtained were reproducible. It has been reported that STAT4 is critical in IFN-α and IFN-β signalling (Darnell, 1997; Frucht *et al.*, 2000). Because STAT4 is absent in STAT4 KO mice, this explains the low expression of IFN-α and IFN-β mRNA. IFN-α, in combination with IL-18, induces IFN-γ expression efficiently in NK cells (Matikainen *et al.*, 2001). Although IL-18 mRNA expression is high in STAT4 KO mice, IFN-α mRNA expression is low. This explains why IFN-γ mRNA expression is also low in STAT4 KO mice.

Alveolar macrophages are not activated in STAT4 KO mice because IFN-γ mRNA expression is low and IFN-γ is unable

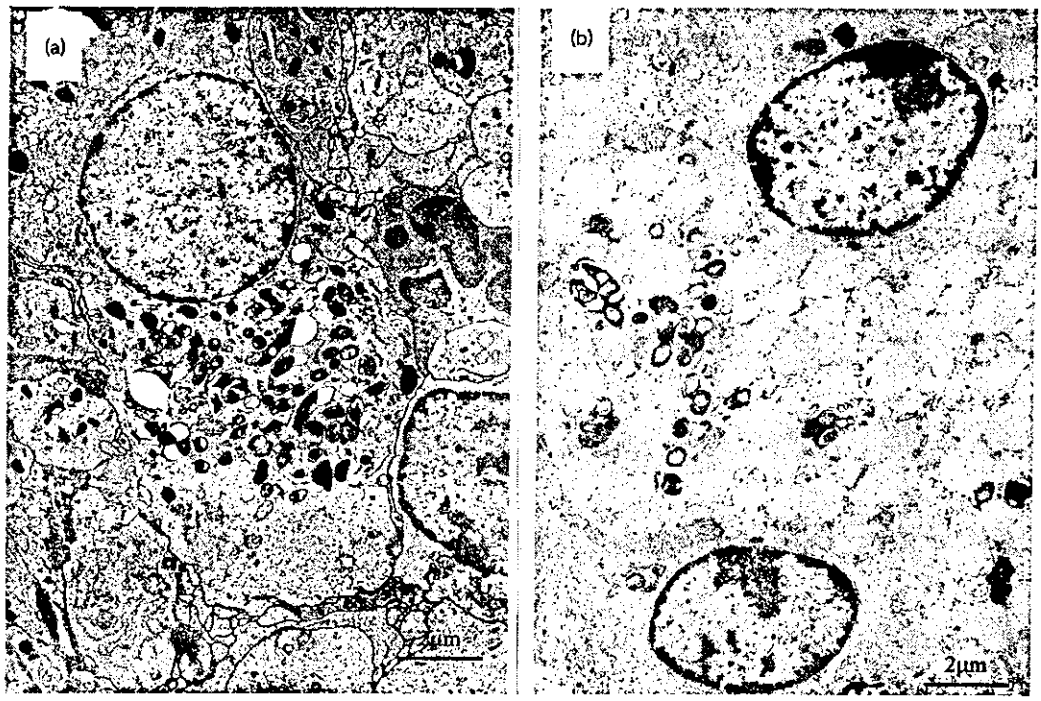

Fig. 2. Electron micrographs of lung lesions from STAT4 KO (a) and WT (b) mice obtained 7 weeks after airborne infection with *M. tuberculosis* Kurono strain. Phagosomes in the STAT4 KO mice contain more tubercle bacilli than those from the WT mice. Bars, 2 μm.

to activate alveolar macrophages. This explains the low expression of iNOS mRNA, the product of which is responsible for production of NO. NO is essential for killing tubercle bacilli and it is known to play an important role in mycobacterial killing mechanisms. It has been reported that, in STAT4 KO mice, induction of IFN-γ expression and activation of NK cells are abrogated, so our present findings are consistent with these observations (Kaplan *et al.*, 1996).

The levels of expression of IL-2, IL-6, IL-12 and IL-18 mRNA were slightly higher in STAT4 KO mice than in WT mice. Although it is known that development of Th1-type T-helper cells is inhibited strongly in STAT4 KO mice, this does not explain the relatively high expression of IL-2, -6, -12 and -18 mRNA (Kaplan *et al.*, 1996). The development of Th1 cells in response to *Listeria monocytogenes*, a common intracellular pathogen, is impaired in the absence of STAT4 (Kaplan *et al.*, 1996), but there have been no reports on cytokine mRNA expression. Further studies will be required to explain this relatively high mRNA expression. The level of IL-12 mRNA expression is rather high in STAT4 KO mice. Therefore, we conclude that T cells from *M. tuberculosis*-infected STAT4 KO mice fail to respond to IL-12 due to impaired IL-12 receptor expression. Susceptibility to *M. tuberculosis* infection is not due to the inability to produce IL-12, rather to a lack of IL-12 responsiveness (Rodriguez-Sosa *et al.*, 2001).

On the other hand, STAT6 KO mice did not develop large pulmonary granulomas, similar to WT mice. STAT6 is activated by IL-4 stimulation. Lymphocytic proliferation in response to IL-4 and the class switch to IgE and Th2-type T-helper cell development are inhibited significantly in STAT6 KO mice (Kaplan *et al.*, 1996). However, Th1-type T-helper cell development is not affected in STAT6 KO mice and IFN mRNA was expressed in STAT6 KO mice (data not shown). It is safe to say that Th2 T-helper cells do not affect *M. tuberculosis*-induced granuloma formation substantially.

There have been two recent reports on the relationship between STAT4 activation and mycobacterial infection (*Mycobacterium leprae* and *Mycobacterium avium*) (Kim *et al.*, 2001; Gollob *et al.*, 2000). IL-12 induced STAT4 phosphorylation and DNA binding in *M. leprae*-activated T cells from tuberculoid patients (Kim *et al.*, 2001). It has also been reported that activation of STAT4 alone is not sufficient for IL-12-induced IFN-γ production and proliferation and that other STAT proteins play a role in responses to IL-12 (Gollob *et al.*, 2000). However, there have been no reports of a role for STAT4 protein in *M. tuberculosis* infection. STAT4 seems to be required for promoting Th1 development and also plays a role in the inhibition of Th2 differentiation in *M. tuberculosis* infection. In the absence of STAT4, T cells are unable to produce IFN-γ or to proliferate in response to IL-12.

In summary, STAT4 KO mice succumbed to *M. tuberculosis* in the late phase of murine tuberculosis. Our data demonstrate that the STAT4-mediated pathway is critical for the development of protective immunity against tuberculosis.

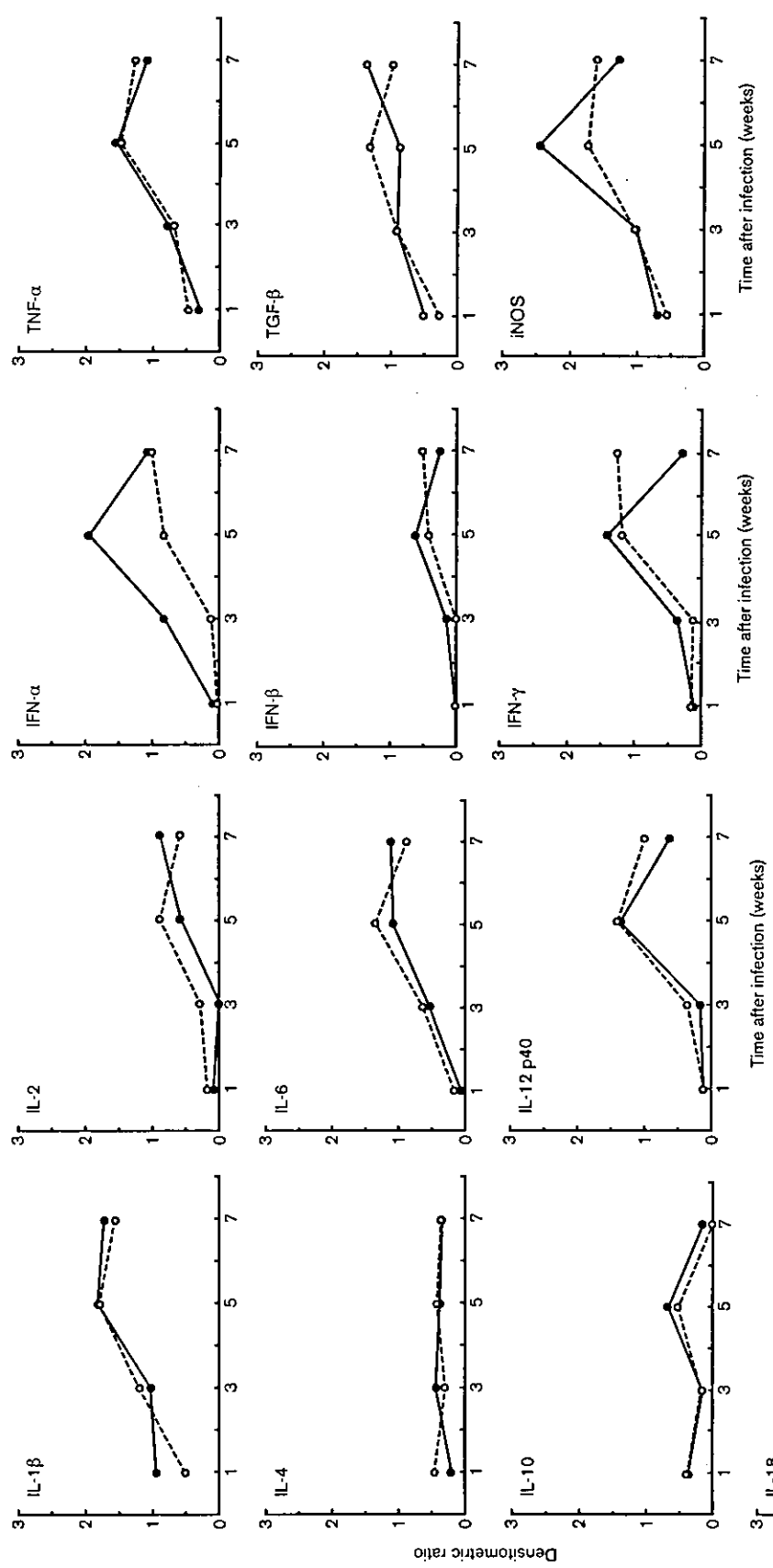

Fig. 3. Densitometric analysis of *in vivo* expression of mRNA for various cytokines, iNOS and TGF-β in STAT4 KO (○, dotted lines) and WT (●, solid lines) mice infected with *M. tuberculosis* Kurono strain. RT-PCR data were obtained and densitometric ratios relative to β-actin mRNA were then obtained using NIH Image.

ACKNOWLEDGEMENTS

This study was supported in part by an International Collaborative Study Grant awarded to I. S. from the Ministry of Health, Labour and Welfare, Japan.

REFERENCES

Cooper, A. M. D., Dalton, D. K., Stewart, T. A., Griffin, J. P., Russell, D. G. & Orme, I. M. (1993). Disseminated tuberculosis in interferon-γ gene-disrupted mice. *J Exp Med* **178**, 2243–2247.

Cooper, A. M., Magram, J., Ferrante, J. & Orme, I. M. (1997). Interleukin 12 (IL-12) is crucial to the development of protective immunity in mice intravenously infected with *Mycobacterium tuberculosis*. *J Exp Med* **186**, 39–45.

Darnell, J. E., Jr (1997). STATs and gene regulation. *Science* **277**, 1630–1635.

Flynn, J. L., Chan, J., Triebold, K. J., Dalton, T. K., Stewart, T. A. & Bloom, B. R. (1993). An essential role for interferon-γ in resistance to *Mycobacterium tuberculosis* infection. *J Exp Med* **178**, 2249–2254.

Flynn, J. L., Goldstein, M. M., Chan, J., Triebold, K. J., Pfeffer, K., Lowenstein, C. J., Schreiber, R., Mak, T. W. & Bloom, B. R. (1995). Tumor necrosis factor-α is required in the protective immune response against *Mycobacterium tuberculosis* in mice. *Immunity* **2**, 561–572.

Frucht, D. M., Aringer, M., Galon, J. & 8 other authors (2000). Stat4 is expressed in activated peripheral blood monocytes, dendritic cells, and macrophages at sites of Th1-mediated inflammation. *J Immunol* **164**, 4659–4664.

Gollob, J. A., Veenstra, K. G., Jyonouchi, H. & 8 other authors (2000). Impairment of STAT activation by IL-12 in a patient with atypical mycobacterial and staphylococcal infections. *J Immunol* **165**, 4120–4126.

Kaneko, H., Yamada, H., Mizuno, S., Udagawa, T., Kazumi, Y., Sekikawa, K. & Sugawara, I. (1999). Role of tumor necrosis factor-α in *Mycobacterium*-induced granuloma formation in tumor necrosis factor-α-deficient mice. *Lab Invest* **79**, 379–386.

Kaplan, M. H., Sun, Y. L., Hoey, T. & Grusby, M. J. (1996a). Impaired IL-12 responses and enhanced development of Th2 cells in Stat4-deficient mice. *Nature* **382**, 174–177.

Kaplan, M. H., Schindler, U., Smiley, S. T. & Grusby, M. J. (1996b). Stat6 is required for mediating responses to IL-4 and for development of Th2 cells. *Immunity* **4**, 313–319.

Kaplan, M. H., Daniel, C., Schindler, U. & Grusby, M. J. (1998). Stat proteins control lymphocyte proliferation by regulating $p27^{Kip1}$ expression. *Mol Cell Biol* **18**, 1996–2003.

Kim, J., Uyemura, K., Van Dyke, M. K., Legaspi, A. J., Rea, T. H., Shuai, K. & Modlin, R. L. (2001). A role for IL-12 receptor expression and signal transduction in host defense in leprosy. *J Immunol* **167**, 779–786.

Kindler, V., Sappino, A. P., Grau, G. E., Piguet, P. F. & Vassalli, P. (1989). The inducing role of tumor necrosis factor in the development of bactericidal granulomas during BCG infection. *Cell* **56**, 731–740.

Matikainen, S., Paananen, A., Miettinen, M., Kurimoto, M., Timonen, T., Julkonen, I. & Saraneva, T. (2001). IFN-α and IL-18 synergistically enhance IFN-γ production in human NK cells: differential regulation of Stat4 activation and IFN-γ gene expression by IFN-α and IL-12. *Eur J Immunol* **31**, 2236–2245.

Rodriguez-Sosa, M., Monteforte, G. M. & Satoskar, A. R. (2001). Susceptibility to *Leishmania mexicana* infection is due to the inability to produce IL-12 rather than lack of IL-12 responsiveness. *Immunol Cell Biol* **79**, 320–322.

Sugawara, I., Yamada, H., Kazumi, Y. & 7 other authors (1998). Induction of granulomas in interferon-γ gene-disrupted mice by avirulent but not by virulent strains of *Mycobacterium tuberculosis*. *J Med Microbiol* **47**, 871–877.

Sugawara, I., Yamada, H., Kaneko, H., Mizuno, S., Takeda, K. & Akira, S. (1999). Role of interleukin-18 (IL-18) in mycobacterial infection in IL-18-gene-disrupted mice. *Infect Immun* **67**, 2585–2589.

Sugawara, I., Mizuno, S., Yamada, H., Matsumoto, M. & Akira, S. (2001). Disruption of nuclear factor-interleukin-6, a transcription factor, results in severe mycobacterial infection. *Am J Pathol* **158**, 361–366.

Sugawara, I., Yamada, H., Mizuno, S., Li, C. Y., Nakayama, T. & Taniguchi, M. (2002). Mycobacterial infection in natural killer T cell knockout mice. *Tuberculosis* **82**, 97–104.

Yamada, H., Mizuno, S., Reza-Gholizadeh, M. & Sugawara, I. (2001). Relative importance of NF-κB p50 in mycobacterial infection. *Infect Immun* **69**, 7100–7105.

Gene Therapy (2003) 10, 272–277

www.nature.com/gt

RESEARCH ARTICLE

Recombinant Sendai virus provides a highly efficient gene transfer into human cord blood-derived hematopoietic stem cells

CH Jin[1], K Kusuhara[1], Y Yonemitsu[2], A Nomura[1], S Okano[2], H Takeshita[2], M Hasegawa[3], K Sueishi[2] and T Hara[1]

[1]*Department of Pediatrics, Graduate School of Medical Sciences, Kyushu University, Fukuoka, Japan;* [2]*Department of Pathology, Division of Pathophysiological and Experimental Pathology, Graduate School of Medical Sciences, Kyushu University, Fukuoka, Japan; and* [3]*DNAVEC Research Inc. Tsukuba, Ibaraki, Japan*

Hematopoietic stem cells (HSCs) are a promising target for gene therapy, however, the low efficiencies of gene transfer using currently available vectors face practical limitations. We have recently developed a novel and efficient gene transfer agent, namely recombinant Sendai virus (SeV), and we have here characterized SeV-mediated gene transfer to human cord blood (CB) HSCs and primitive progenitor cells (PPC) using the jelly fish green fluorescent protein (GFP) gene. Even at a relatively low titer (10 multiplicity of infections), SeV achieved highly efficient GFP expression in CB CD34⁺ cells (85.5 ± 5.8%), as well as more immature CB progenitor cells, CD34⁺AC133⁺ (88.2 ± 3.7%) and CD34⁺CD38⁻ (84.6 ± 5.7%) cells, without cytokines prestimulation, that was a clear contrast to the features of gene transfer using retroviruses. SeV-mediated gene transfer was not seriously affected by the cell cycle status. In vitro cell differentiation studies revealed that gene transfer occurred in progenitor cells of all lineages (GM-CFU, 73.0 ± 11.1%; BFU-E, 24.7 ± 4.0%; Mix-CFU, 59 ± 4.0%; and total, 50.0 ± 7.0%). These findings show that SeV could prove to be a promising vector for efficient gene transfer to CB HSCs, while preserving their ability to reconstitute the entire hematopoietic series.
Gene Therapy (2003) **10**, 272–277. doi:10.1038/sj.gt.3301877

Keywords: *Recombinant Sendai virus; cord blood; hematopoietic stem cells; CD34⁺ cells; gene therapy*

Introduction

Gene therapy targeting hematopoietic stem cells (HSCs) holds promise to treat a number of genetic and acquired diseases. HSCs are an ideal target on this purpose, because these progenitors can reconstitute the entire hematopoietic system in a recipient during a lifetime. Successful application of stem-cell-based gene therapies to treat blood system disorders requires an efficient gene delivery system, long-term reconstitution of hematopoiesis from transduced HSCs, and stable expression of the therapeutic gene(s) in the affected blood cell lineages. Although a number of experimental studies have been done for gene transfer to HSCs, a major limitation of currently available gene transfer vectors is the low gene transfer efficiency.

We recently developed a novel viral vector for efficient gene transfer, namely recombinant Sendai virus (SeV), through which there is an efficient gene transfer into several systems, including airway epithelial cells,[1] vascular tissue,[2] skeletal muscle,[3] as well as synovial cells.[4] SeV, a member of the family *Paramyxoviridae*, has a non-segmented negative-strand RNA genome and makes use of sialic acid residue on surface glycoprotein or asialoglycoprotein present on most cell types as a receptor.[5] As SeV uses a cytoplasmic transcription system, it can mediate gene transfer to a cytoplasmic location.[6] There are technical advantages in the use of recombinant SeV as gene therapy vector. First, the activity of SeV particles is stable and can be easily concentrated to high titers, which is in clear contrast to the features of retroviral vectors. Second, and most importantly, the modalities of target cell processing and viral transduction are technically non-demanding and feasible in clinical situations that require tranduction into large numbers of target cells.

Since characteristics of gene transfer with SeV to HSCs have not been documented yet, we analyzed the efficiency and transgene expression in SeV-mediated gene transfer to cord blood (CB) hematopoietic precursor and progenitor cells to test whether SeV could overcome current limitations in gene transfer for HSC.

Correspondence: K Kusuhara, Department of Pediatrics, Graduate School of Medical Sciences, Kyushu University, 3-1-1, Maidashi, Higashi-ku, Fukuoka 812-8582, Japan
Received 9 April 2002; accepted 1 August 2002

Results

Transduction efficiency in CB CD34⁺ cells

We first evaluated the efficiency of recombinant SeV vector-mediated gene transfer to CB CD34⁺cells. Evaluated based on green fluorescent protein (GFP)

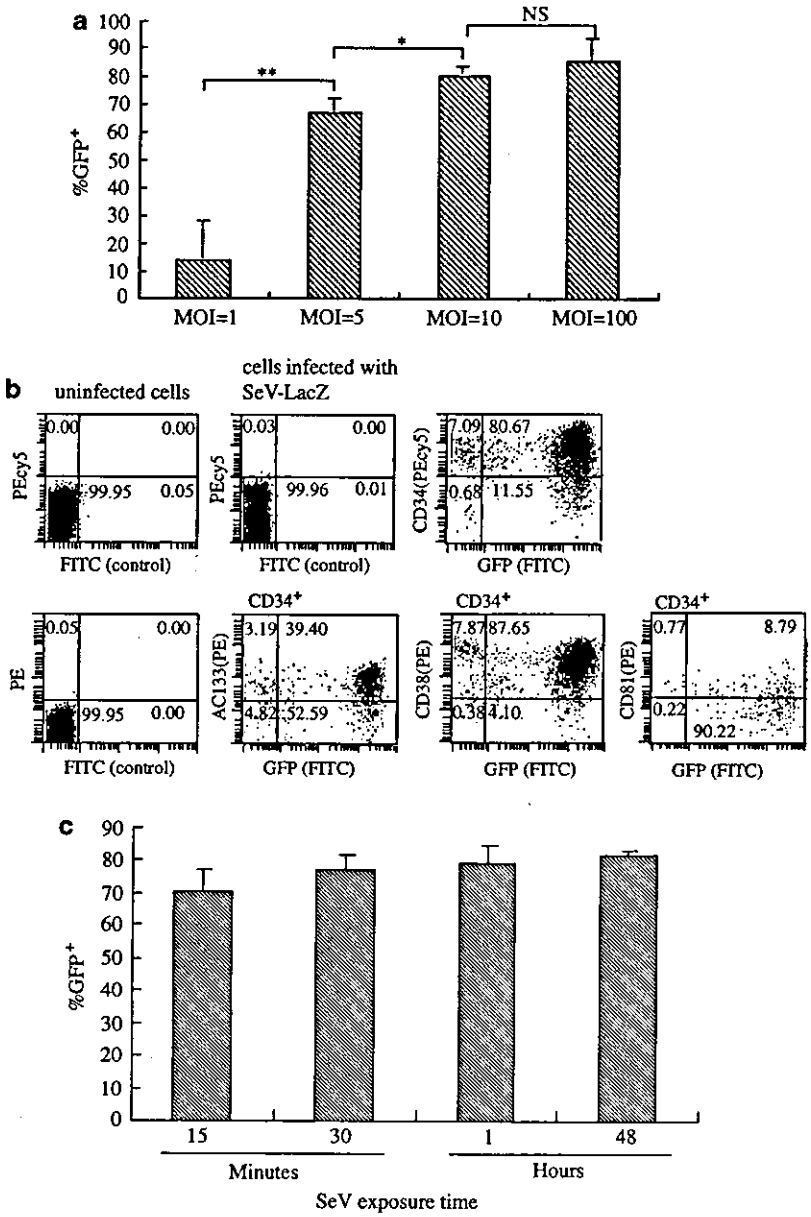

*Figure 1 (a) SeV-mediated, dose-dependent GFP gene transfer to human CB-derived CD34⁺ cells. After enrichment of CD34⁺ cells using microbeads bound to anti-human CD34 antibody, the vector solution with SeV-GFP at each titer was simply added to the cell suspension. Forty-eight hours later, the cells were subjected to flow-cytometric analyses. The bar graph indicates the dose-dependent increase in gene transfer efficiency, and the efficiency almost reached its peak at 10 multiplicity of infections (MOI=10). Data from four CB samples, each in triplicate, are shown as mean ± standard deviation values.**$P<0.01$. *$P<0.05$. NS: not significant. (b) Flow-cytometric analysis indicating SeV-mediated, efficient gene transfer to immature CD34⁺ precursors (CD34⁺AC133⁺, CD34+CD38⁻ and CD34⁺CD81⁺ cells). Forty-eight hours after gene transfer at MOI=10 with SeV-GFP to each subpopulation, the cells were subjected to flow-cytometric analysis. The experiment was done in triplicate, with consistent results. (c). Effect of vector exposure time on SeV-mediated gene transfer into enriched CB CD34⁺ cells. Enriched CB CD34⁺ cells were exposed to SeV-GFP (MOI=10) by adding vector solution, and the cells were washed twice with fresh media after the respective incubation time. Forty-eight hours after the addition of vector solution, cells were subjected to flow-cytometric analysis. Data, each in triplicate, are shown as mean ± standard deviation values.*

expression, using flow cytometry on day 2, CB CD34⁺cells showed a dose-dependent, highly efficient GFP gene transduction rate with a plateau at the titer of 10 multiplicity of infections (MOI) and over (Figure 1a). Transduction in the following experiments was thus done at the titer of 10 MOI. As shown in Figure 1b, highly efficient expression of transgene on day 2 was observed not only in CB CD34⁺ cells (85.5 ± 5.8%), but also in more immature CB progenitors, CD34⁺AC133⁺ (88.2 ± 3.7%) and CD34⁺CD38⁻ (84.6 ± 5.7%) cells, and multilymphoid progenitor, CD34⁺CD81⁺ cells (87.3±4.7%).

Next, we evaluated the effect of vector exposure time on SeV-mediated gene transfer efficiency at the titer of MOI=10. The GFP gene expression on day 2 was not markedly affected by vector–cell interaction time, and even a 30-min exposure led to a GFP expression level comparable to that seen with a 48-h exposure (Figure 1C).

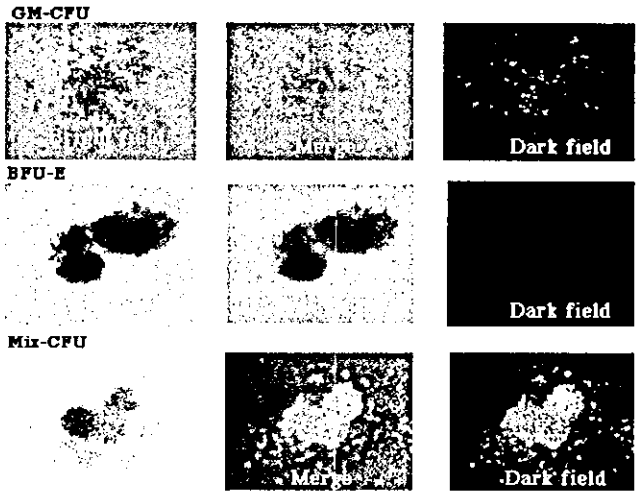

Figure 2 Colony assays for human cord blood-derived CD34⁺ cells treated by SeV-GFP. Representative fluorescence microscopic data on GFP expression of colonies from CB CD34⁺ cells. All cell lineages, including GM-CFU (upper series) and BFU-E (middle series) as well as Mix-CFU (bottom series), showed efficient GFP expression.

Transduction of CB-derived CFUs

To evaluate the gene transfer potential of the SeV vector to colony-forming CB progenitors, colony assays were done for CB CD34⁺ cells exposed to SeV. GFP expression on day 14 was analyzed in colonies derived from committed CFUs. Highly efficient GFP expression was observed in progenitor cells of all lineages (GM-CFU, 73.0 ± 11.1%; BFU-E, 24.7 ± 4.0%; Mix-CFU, 59 ± 4.0%; Total, 50.0 ± 7.0%) (Figure 2 and Table 1). Although the total number of colonies derived from SeV-treated CB CD34⁺ cells tended to be smaller (P=0.09) than those from control CB CD34⁺ cells, the numbers of GM-CFU, BFU-E and Mix-CFU colonies were almost the same (Table 1), thereby suggesting that the transduction procedure did not significantly impair growth of these colonies.

Efficiency of transduction relative to cell cycle status

To investigate the dependency of transduction efficiency with SeV on the cell cycle phases, we analyzed the distribution of transduced CB CD34⁺ cells in each subcompartment of the cell cycle. Cell cycle fractionation was defined by three-color flow-cytometric analysis of transduced CB CD 34⁺ cells stained with 7-AAD and Ki-67. We found that GFP was expressed in all phases of the cell cycle: 22.64 ± 6.12% of G_0, 78.32 ± 6.83% of G_1, and 83.05 ± 2.73% of $S/G_2/M$ CB cells (Figure 3a). Similar results were obtained in CB CD34⁺ cells treated with aphidicolin (Figure 3b).

Table 1 Quantitative analysis of GFP expression in colony-forming cells (CFCs) from cord blood CD34⁺ cells by progenitor colony assay

		Total	GM-CFU	BFU-E	Mix-CFU
		GFP⁺/total (%)	GFP⁺/total (%)	GFP⁺/total (%)	GFP⁺/total (%)
CB1	SeV+	83/198 (41.9)	51/72 (70.8)	16/81 (19.8)	3/5 (60)
	SeV−	0/270	0/72	0/98	0/10
CB2	SeV+	138/258 (53.5)	75/90 (83.3)	36/123 (29.3)	6/11 (54.5)
	SeV−	0/320	0/150	0/110	0/6
CB3	SeV+	124/224 (55.4)	75/100 (75)	16/66 (24.2)	5/8 (62.5)
	SeV−	0/260	0/110	0/95	0/13

SeV+: transfected by SeV-GFP. SeV−: control.
Numbers of colonies per 2000 cells.

Effect of SeV-mediated gene transfer on HSCs proliferation.

To evaluate the proliferative activity of transduced CB CD34⁺ cells, short-term liquid cultures were observed after exposure to the SeV vector. As shown in Figure 4a, the growth of CB CD34⁺ cells exposed to the SeV vector was dose-dependently inhibited with no significant difference among MOI=5, 10 and 100. When cell viabilities on days 2, 6 and 10 were compared between SeV-treated and control CB CD34⁺ cells, SeV-treated cells showed the lowest viability on day 6 (Figure 4b). Annexin V-positive rates of CB CD34⁺ cells treated with SeV at MOI=10 and control CB CD34⁺ cells were 10% and 2% respectively, on day 4 (data not shown). Absolute numbers of four subpopulations ($CD34^+GFP^+$, $CD34^+GFP^-$, $CD34^-GFP^+$ and $CD34^-GFP^-$ cells) in SeV-treated CB CD34⁺ cells at days 2, 6 and 10

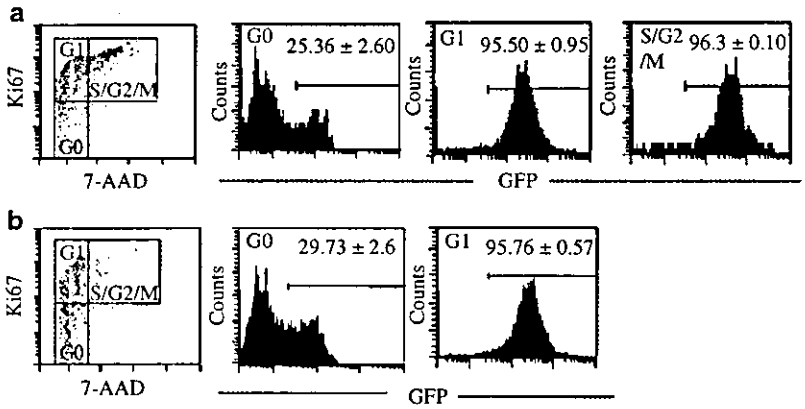

Figure 3 Relationship between cell cycle status and efficiency of transduction with SeV. The percentages of cells with GFP expression in G_0, G_1, and $S/G_2/M$ phases of the cell cycle are shown as mean ± standard deviation values. A representative flow-cytometric data from three experiments is presented: (a) No treatment; (b) progression of transduced cells from G1/S boundary to S phase was blocked by aphidicolin treatment.

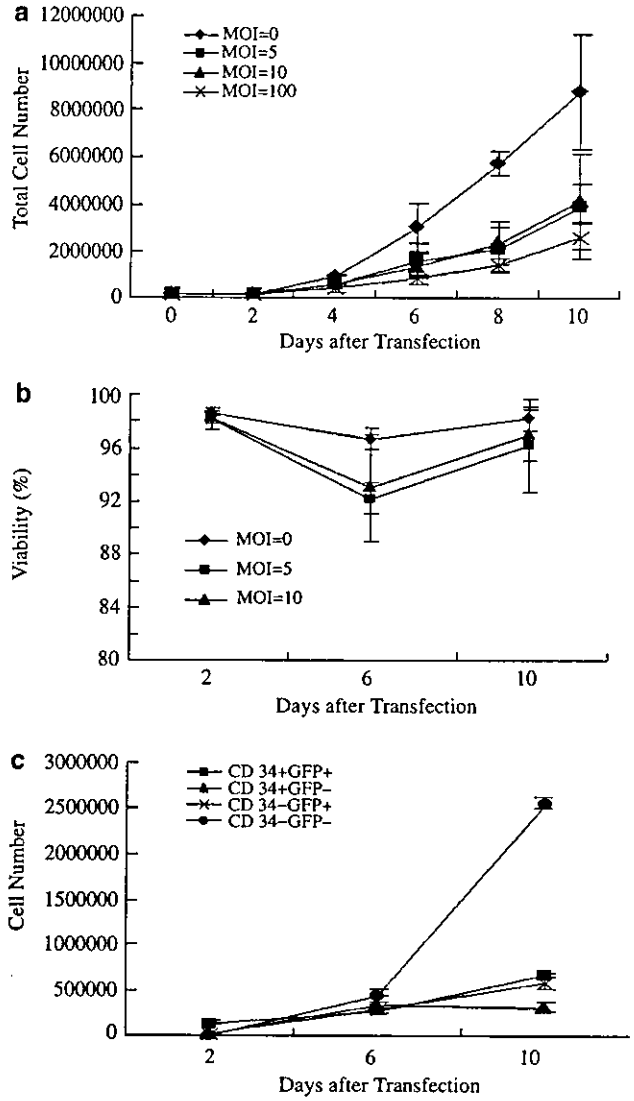

Figure 4 Effect of SeV infection on the proliferative activity of cord blood CD34⁺ cells. CD34⁺cells were transduced with GFP gene by SeV vector at titers 0, 5, 10 and 100 MOIs: (a) the total cell number; (b) viability (MOI=0, 5, 10) and (c) absolute number of four subpopulations (CD34⁺GFP⁺, CD34⁺GFP⁻, CD34⁻GFP⁺ and CD34⁻GFP⁻ cells) were counted at each time point (MOI=10). Data from four cord blood samples, each in triplicate, are shown as mean ± standard deviation values.

are shown in Figure 4c. Although the proliferation of $CD34^-GFP^-$ cells was prominent, $CD34^+GFP^+$ cells continued to grow during the culture period.

Discussion

In the present study, we demonstrated that SeV vector efficiently transferred the GFP gene to $CD34^+$ cell and $CD34^+$ cell subpopulations derived from CB (Figures 1a and b). Transduction efficiency was not seriously affected by the cell cycle status of the CB. In addition, efficient and stable gene expression was observed in clonogenic erythroid, myeloid or mixed progenitor cells (Figure 2 and Table 1). These data show the efficient gene transfer potential of SeV to quiescent cells as well as dividing cells, including HSCs and various differentiated hematopoietic lineages.

Non-dividing $CD34^+$ cells are considered to include the most long-term subsets of HSCs.[7] The quiescent stage of $CD34^+$ cells is important because induction of cell proliferation is associated with a loss of the potential to reconstitute hematopoiesis and with changes in the expression of cellular receptors.[8–10] In this regard, application of retroviruses to HSCs is limited, because efficient gene transfer is only seen in actively replicating target cells. In a retrovirus system, the fraction of dividing cells needs to be expanded before transduction by prestimulation with cytokines in order to increase the transduction efficiency of HSCs up to 40%.[11–13] In the present study, we found that efficient gene transfer with SeV (>80%) was attained without prestimulation of $CD34^+$ cells with cytokines (Figure 1a). Furthermore, the high expression of the GFP gene (25%) in G_0 compartment of $CD34^+$ cells seen with SeV-mediated gene transduction (Figures 3a and b) was comparable to that noted in lentivirus-mediated gene transfer.[14] These results suggest that resting progenitors, long-term culture-initiating cells (LTC-IC) and SCID-repopulating cell (SRC), are easily transduced by the SeV vector with minimal loss of their potential to repopulate, because they are highly enriched in the G_0 compartment.[7, 15] In this regard, the SeV vector is a suitable vehicle for transferring genes into HSCs.

From a clinical point of view, in contrast to retrovirus and lentivirus vectors, SeV-mediated gene transfer to CB $CD34^+$ cells requires only simple procedures. As shown in Figure 1c, $CD34^+$ cells were efficiently transduced by simply adding SeV vector solutions at the titer of MOI=10 with only brief contact time, as noted with other cell types.[1,2] This simplicity in gene transfer procedures using SeV is also advantageous for clinical application to CB HSCs with their capacity to reconstitute the entire hematopoietic system.

The potential cytotoxicity of SeV to the target cell remains to be a concern, because SeV induces cytopathic effects in some cells, including CV-1 cells.[16] In the present study, growth inhibition of transduced $CD34^+$ cells was observed in our short-time liquid suspension culture. Since SeV-induced apoptosis might be possible in some permissive cells through activation of caspase 3 and caspase 8,[17] we here assessed the accumulation of annexin V. As the annexin V-positive rate of SeV-treated $CD34^+$ cells (10%) was higher than that of control $CD34^+$ cells (2%) on day 4 and SeV-treated cells showed the lowest viability on day 6 (Figure 4b), the induction of apoptosis appears to contribute, probably in part, to decreased cell number. To minimize the damage of transduced cells, development of an SeV vector lacking cytotoxicity-associated genes such as C gene might be needed. In contrast, the formation of progenitor colonies, such as GM-CFU, BFU-E and Mix-CFU, in semi-solid culture was not significantly affected after transduction with SeV (Figure 2 and Table 1). The discrepancy may be explained by the possibility that $CD34^+$ cells infected with SeV at the very early stage of hematopoietic differentiation was less sensitive to growth inhibition than those infected thereafter. Therefore, it is necessary to evaluate *in vivo* survival, proliferation and transgene expression of CB $CD34^+$ cells transduced with SeV.

In summary, although further *in vivo* reconstruction studies are needed, the SeV vector is an important candidate for gene transfer to HSCs due to its potential for superior gene transfer into HSCs.

Materials and methods

Construction of SeV-GFP

SeV-GFP was constructed, as described.[18,19] In brief, 18 bp of spacer sequence 5′-(G)-CGGCCGCAGATCTT-CACG-3′ with a *NotI* restriction site were inserted between the 5′ non-translated region and the initiation codon of the nucleoprotein (N) gene. This cloned SeV genome also contains a self-cleaving ribosome site from the antigenomic strand of the hepatitis delta virus. The entire cDNA coding *jelly fish* enhanced GFP was amplified by PCR, using primers with a *NotI* site and new sets of SeV E and S signal sequence tags for an exogenous gene, then inserted into the *NotI* site of the cloned genome. The entire length of the template SeV genome, including exogenous genes, was arranged in multiples of six nucleotides (the so-called 'rule of six').[20] Template SeV genome with an exogenous gene and plasmids encoding N, P, and L proteins (plasmid pGEM-N, pGEM-P, and pGEM-L) was complexed with commercially available cationic lipids, then cotransfected with vaccinia virus vT7-3 into CV-1 or LLMCK cells.[21] Forty hours later, the cells were disrupted by three cycles of freezing and thawing and injected into the chorioallantoic cavity of 10-day-old embryonated chicken eggs. Subsequently, the virus was recovered and the vaccinia virus was eliminated by a second propagation in eggs. Virus titer was determined by hemagglutination assay, using chicken red blood cells,[22] and the virus was stored at −80°C until use.

CB cells samples

Heparinized CB samples were obtained from umbilical cord veins of four full-term human newborns without hereditary disorders or hematological abnormalities and were analyzed within 24 h. All samples were collected after written informed consent was obtained from the parents.

CD34⁺ cell selection and gene transfer

CB CD34 cells were labeled with hapten-conjugated monoclonal antibodies (mAbs) against human CD34 (clone QBEnd/10), followed by an anti-hapten antibodies (Abs) coupled with microbeads. The bead-positive cells (CD34 cells) were enriched on positive-selection columns set in a magnetic field. Flow-cytometric analysis of purified cells using a different clone of FITC-conjugated anti-CD34 mAb showed more than 95% purity. Purified CD34⁺ cells were then suspended at 2 to 4×10^5 cells/ml in 2.5-cm tissue culture dishes in serum-free Iscove's Modified Dulbecco's medium (IMDM) containing 30% fetal bovine serum (FBS), 10 ng/ml of stem cell factor (SCF, Kirin Brewery Company, Tokyo, Japan), interleukin 6 (IL-6, Kirin Brewery Co), and thrombopoietin (TPO, Kirin Brewery Co). In all experiments, gene transfer was carried out by adding various amounts of vector solution to the media. Cells were then incubated at 37°C in a 5% CO_2 incubator, and collected for cell count and flow-cytometric analysis at different time points, as indicated in Figures 1 and 4. To evaluate the effect of vector exposure time on SeV-mediated gene transfer, cells were washed twice with fresh media after treatment with SeV at MOI=10. Except for this experiment, the washing after transduction was omitted for purposes of simplification.

Colony assays

To determine the number of erythroid, myeloid, mixed lineage progenitors, 2000 of the transduced cells were plated in 35-mm tissue culture dishes containing 1 mL of 0.88%. methylcellulose-based semi-solid culture medium supplemented with 30% FBS, 50 U/ml of interleukin 3 (IL-3, Kirin Brewery Co.), 50 ng/ml of SCF, 50 ng/ml of granulocyte-macrophage-colony-stimulating factor (GM-CSF, Kirin Brewery Co.), and 10 U/ml of erythropoietin (EPO, Kirin Brewery Co.). After 14 days of incubation at 37°C in a 5% CO_2 incubator, colony-forming units-granulocyte-macrophage (CFU-GM), burst-forming units-erythroid (BFU-E), colony-forming units-granulocyte erythrocyte monocyte macrophage (CFU-Mix) colonies were enumerated and GFP-expressing colonies were identified, using a fluorescence microscope.

Flow-cytometric analysis

Transduced cells were stained with appropriate amounts of phycoerythrin (PE)- and phycoerythrin 5.1(PC-5)-conjugated mAbs at 4°C for 20 min. All mAbs were obtained from Coulter-Immunotech (Miami, FL, USA). The cells were washed twice and suspended in phosphate-buffered saline (PBS). Flow-cytometric analysis was done using EPICS XL (Beckman-Coulter, Hialeah, FL, USA). A total of at least 10 000 events were analyzed for each sample. Gates were set according to forward and side scatters. Cell viability and annexin V-positive rate were assessed by 7-AAD staining and by annexin V-FITC (MBL, Nagoya, Japan) staining, respectively.

For cell cycle analysis, cells were analyzed for Ki-67 expression and DNA content as described by Jordan *et al*,[23] but with minor modifications. Briefly, cells incubated at 37°C in a 5% CO_2 incubator for 48 h after transduction were washed and resuspended in 1-ml PBS containing 0.4% formaldehyde. After 30 min incubation at 4°C, 1 ml of PBS containing 0.2% Triton X-100 was added and cells were left overnight at 4°C. Cells were then washed twice in PBS containing 1% bovine serum albumin (BSA) and stained with PE-conjugated anti-Ki-67 (clone MIB-1; Immunotech, West-brook, ME, USA) for 60 min at 4°C. Isotype-matched mAb control was used in parallel. Finally, cells were washed and resuspended in PBS containing 1% BSA and 5 μg/ml 7-aminoactinomycin-D (7-AAD; Sigma). After 3 h of incubation on ice, samples were run on flow cytometer using FL-1 and FL-2 channels for Ki-67 and 7-AAD, respectively. To block the cells at G1/S boundary, transduced cells were treated with 2 mg/ml of aphidicolin (Sigma Chemical Co, St Louis, MO, USA) at 37°C in a 5% CO_2 incubator for 48 h.

Acknowledgements

We thank Dr Kusuo Sanada for providing cord blood samples. This study was supported by a Grant of Promotion of Basic Scientific Research in Medical Frontier of the Organization for Pharmaceutical Safety

and Research, and by a Grant-in-Aid for Scientific Research from the Ministry of Education, Culture, Sports, Science and Technology of Japan. M Ohara provided language assistance.

References

1 Yonemitsu Y *et al.* Efficient gene transfer to airway epithelium using recombinant Sendai virus. *Nat Biotechnol* 2000; **18**: 970–973.
2 Masaki I *et al.* Recombinant Sendai virus-mediated gene transfer to vasculature: a new class of efficient gene transfer vector to the vascular system. *FASEB J* 2001; **15**: 1294–1296.
3 Shiotani A *et al.* Skeletal muscle regeneration after insulin-like growth factor I gene transfer by recombinant Sendai virus vector. *Gene Ther* 2001; **8**: 1043–1050.
4 Yamashita A *et al.* Fibroblast growth factor-2 determines severity of joint disease in adjuvant-induced arthritis in rats. *J Immunol* 2002; **168**: 450–457.
5 Markwell MA, Svennerholm L, Paulson JC. Specific gangliosides function as host cell receptors for Sendai virus. *Proc Natl Acad Sci USA* 1981; **78**: 5406–5410.
6 Moyer SA, Baker SC, Lessard JL. Tubulin: a factor necessary for the synthesis of both Sendai virus and vesicular stomatitis virus RNAs. *Proc Natl Acad Sci USA* 1986; **83**: 5405–5409.
7 Gothot A *et al.* Assessment of proliferative and colony-forming capacity after successive *in vitro* divisions of single human CD34+ cells initially isolated in G_0. *Exp Hematol* 1998; **26**: 562–570.
8 Becker PS *et al.* Adhesion receptor expression by hematopoietic cell lines and murine progenitors: modulation by cytokines and cell cycle status. *Exp Hematol* 1999; **27**: 533–541.
9 Gonzalez R *et al.* Increased gene transfer in acute myeloid leukemic cells by an adenovirus vector containing a modified fiber protein. *Gene Ther* 1999; **6**: 314–320.
10 Huang S, Endo RI, Nemerow GR. Upregulation of integrins alpha v beta 3 and alpha v beta 5 on human monocytes and lymphocytes facilitates adenovirus-mediated gene delivery. *J Virol* 1995; **69**: 2257–2263.
11 Bodine DM, McDonagh KT, Seidel NE, Nienhuis AW. Survival and retrovirus infection of murine hematopoietic stem cells *in vitro*: effects of 5-FU and method of infection. *Exp Hematol* 1991; **19**: 206–212.
12 Tumas DB *et al.* High-frequency cell surface expression of a foreign protein in murine hematopoietic stem cells using a new retroviral vector. *Blood* 1996; **87**: 509–517.
13 Cavazzana-Calvo M *et al.* Gene therapy of human severe combined immunodeficiency (SCID)-X1 disease. *Science* 2000; **28**: 669–672.
14 Luther-Wyrsch A *et al.* Stable transduction with lentiviral vectors and amplification of immature hematopoietic progenitors from cord blood of preterm human fetuses. *Hum Gene Ther* 2001; **12**: 377–389.
15 Gothot A *et al.* Cell cycle-related changes in repopulating capacity of human mobilized peripheral blood $CD34^+$ cells in non-obese diabetic/severe combined immune-deficient mice. *Blood* 1998; **92**: 2641–2649.
16 Kato A *et al.* The paramyxovirus, Sendai virus, V protein encodes a luxury function required for viral pathogenesis. *EMBO J* 1997; **16**: 578–587.
17 Bitzer M *et al.* Sendai virus infection induces apoptosis through activation of caspase-8 (FLICE) and caspase-3 (CPP32). *J Virol* 1999; **73**: 702–708.
18 Kato A *et al.* Initiation of Sendai virus multiplication from transfected cDNA or RNA with negative or positive sense. *Genes Cells* 1996; **1**: 569–579.
19 Sakai Y *et al.* Accommodation of foreign genes into the Sendai virus genome: sizes of inserted genes and viral replication. *FEBS Lett* 1999; **456**: 221–226.
20 Kolakofsky D *et al.* Paramyxovirus RNA synthesis and the requirement for hexamer genome length: the rule of six revisited. *J Virol* 1998; **7**: 891–899.
21 Fuerst TR, Niles EG, Studier FW, Moss B. Eukaryotic transient-expression system based on recombinant vaccinia virus that synthesizes bacteriophage T7 RNA polymerase. *Proc Natl Acad Sci USA* 1986; **83**: 8122–8126.
22 Yonemitsu Y, Kaneda Y. Hemagglutinating virus of Japan-liposome-mediated gene delivery to vascular cells. In: Baker AH (ed.). *Molecular Biology of Vascular Diseases. Methods in Molecular Medicine.* Humana Press: Clifton, 1999, pp 295–306.
23 Jordan CT, Yamasaki G, Minamoto D. High-resolution cell cycle analysis of defined phenotypic subsets within primitive human hematopoietic cell populations. *Exp Hematol* 1996; **24**: 1347–1355.

The Roles of Toll-Like Receptor 9, MyD88, and DNA-Dependent Protein Kinase Catalytic Subunit in the Effects of Two Distinct CpG DNAs on Dendritic Cell Subsets[1]

Hiroaki Hemmi,*† Tsuneyasu Kaisho,*†‡ Kiyoshi Takeda,*† and Shizuo Akira[2]*†

Oligodeoxynucleotides containing unmethylated CpG motifs (CpG DNAs) can function as powerful immune adjuvants by activating APC. Compared with conventional phosphorothioate-backbone CpG DNAs, another type of CpG DNAs, called an A or D type (A/D-type), possesses higher ability to induce IFN-α production. Conventional CpG DNAs can exert their activity through Toll-like receptor 9 (TLR9) signaling, which depends on a cytoplasmic adapter, MyD88. However, it remains unknown how A/D-type CpG DNAs exhibit their immunostimulatory function. In this study we have investigated murine dendritic cell (DC) responses to these two distinct CpG DNAs. Not only splenic, but also in vitro bone marrow-derived, DCs could produce larger amounts of IFN-α in response to A/D-type CpG DNAs compared with conventional CpG DNAs. This IFN-α production was mainly due to the B220$^+$ DC subset. On the other hand, the B220$^-$ DC subset responded similarly to both CpG DNAs in terms of costimulatory molecule up-regulation and IL-12 induction. IFN-α, but not IL-12, induction was dependent on type I IFN. However, all activities of both CpG DNAs were abolished in TLR9- and MyD88-, but were retained in DNA-PKcs-deficient DCs. This study demonstrates that the TLR9-MyD88 signaling pathway is essential for all DC responses to both types of CpG DNAs. ***The Journal of Immunology*****, 2003, 170: 3059–3064.**

Bacterial DNA can stimulate innate immunity in mammals (1–3). This immunostimulatory activity depends on the unmethylated CpG motif, which is abundantly present in microbes. Synthetic oligodeoxynucleotides containing the unmethylated CpG motif (CpG DNAs) are equivalent to bacterial DNA in the immunostimulatory activity. CpG DNAs can induce splenic B cell proliferation, dendritic cell (DC)[3] maturation, and cytokine production from a variety of immune cells (1–3). These CpG DNAs are phosphorothioate-modified oligodeoxynucleotides called K-type CpG DNAs or CpG-B (conventional CpG DNAs). Through the screening of a variety of CpG DNAs, another type of CpG DNAs with a distinct function was identified (4–7). These are termed D-type CpG DNAs or CpG-A (A/D-type CpG DNAs) and are structurally different from conventional CpG DNAs because they carry a phosphorothioate-modified polyguanosine (polyG) stretch at the 5′ and 3′ ends and a phosphodiester backbone CpG motif at the central position. The function of A/D-type CpG DNAs has been extensively characterized in the human system (4, 5). A/D-type CpG DNAs can induce cytokine production in a variety of cells, but exhibit weaker ability to induce proliferation and IgM production of splenocytes than conventional CpG DNAs (4). Notably, A/D-type CpG DNAs have greater ability to induce IFN-α production from plasmacytoid DC (PDC) and IFN-γ from NK cells (5, 6).

We previously demonstrated that Toll-like receptor 9 (TLR9) is essential for CpG DNA-induced immune responses based on the fact that TLR9-deficient (TLR9$^{-/-}$) mice are refractory to CpG DNAs (8). In addition, TLR9 expression is sufficient to confer responsiveness to CpG DNA on a human kidney cell line (9, 10). Some CpG DNAs can activate human immune cells more efficiently than murine ones, while others can activate murine cells more effectively than human ones. This species-specific response is reconstituted by the expression of human or murine TLR9 on an otherwise refractory cell line, suggesting that TLR9 is also critical for the species-specific function of CpG DNAs (9). However, because all these experiments were performed with conventional CpG DNAs, the cellular and molecular mechanisms of how immune cells are activated by A/D-type CpG DNAs remain unelucidated.

In this study we have investigated how these CpG DNAs activate DCs, which play crucial roles in host defense by linking innate and adaptive immunities. Both types of CpG DNAs could induce IL-12 secretion from DCs. However, compared with conventional CpG DNAs, A/D-type CpG DNAs could induce greater amounts of IFN-α production from DCs. A B220$^+$ DC subset, which is considered to be a murine counterpart of human PDC, was mainly responsible for IFN-α production induced by CpG DNAs. Both conventional and A/D-type CpG DNAs required the TLR9 signaling system and could induce IFN regulatory factor 7 (IRF7) mRNA up-regulation at similar levels. Thus, common signaling pathways are involved in the effects of distinct types of CpG DNAs on murine DC subsets.

*Department of Host Defense, Research Institute for Microbial Diseases, Osaka University, and †Solution-Oriented Research for Science and Technology, Japan Science and Technology Corp., Suita, Osaka, Japan; and ‡RIKEN Research Center for Allergy and Immunology, Yokohama, Kanagawa, Japan

Received for publication November 8, 2002. Accepted for publication January 15, 2003.

The costs of publication of this article were defrayed in part by the payment of page charges. This article must therefore be hereby marked *advertisement* in accordance with 18 U.S.C. Section 1734 solely to indicate this fact.

[1] This work was supported by grants from the Ministry of Education, Culture, Sports, Science, and Technology in Japan, and SORST of Japan Science and Technology Corp. H.H. is a Research Fellow of the Japan Society for the Promotion of Science.

[2] Address correspondence and reprint requests to Dr. Shizuo Akira, Department of Host Defense, Research Institute for Microbial Diseases, Osaka University, 3-1 Yamada-oka, Suita, Osaka 565-0871, Japan. E-mail address: sakira@biken.osaka-u.ac.jp

[3] Abbreviations used in this paper: DC, dendritic cell; BM, bone marrow; CpG DNA, oligodeoxynucleotides containing the unmethylated CpG motif; DNA-PKcs, DNA-dependent protein kinase catalytic subunit; Flt3L, Flt3 ligand; IRF7, IFN regulatory factor 7; PDC, plasmacytoid DC; polyG, polyguanosine; SR-A, scavenger receptor A; TLR, Toll-like receptor.

0022-1767/03/$02.00

Materials and Methods

Mice

C57BL/6J mice were purchased from CLEA Japan, Inc. (Tokyo, Japan). MyD88-deficient (MyD88$^{-/-}$) mice were established as described previously (11) and backcrossed over eight times with C57BL/6 mice. TLR9$^{-/-}$ mice were generated as described previously (8). DNA-dependent protein kinase catalytic subunit-deficient (DNA-PKcs$^{-/-}$) mice were provided by Dr. F. W. Alt (Harvard Medical School, Boston, MA) (12). IFN-α/βR-deficient (IFN-α/βR$^{-/-}$) mice were purchased from B&K Universal Ltd. (Hull, U.K.).

Reagents and Abs

Synthesized oligodeoxynucleotides were purchased from Hokkaido System Science (Sapporo, Japan). The sequences and backbones of oligodeoxynucleotides are: ODN1668, tccatgacgttcctgatgct (13); D19, ggTGC ATCGATGCAgggggG (4); and control D, ggTGCATGCATGCAgggggG (4). Capital and lowercase letters in parentheses indicate bases with phosphodiester and phosphorothioate-modified backbones, respectively. Abs against mouse CD11c (clone HL3), CD40 (clone 3/23), CD86 (clone GL1), and B220 (clone RA3-6B2) were purchased from BD PharMingen (San Diego, CA)

Preparation of DCs

To prepare splenocytes containing DCs, spleens were cut unto small fragments and incubated with RPMI 1640 medium containing 400 U/ml collagenase (Wako Pure Chemical Industries, Osaka, Japan) and 15 μg/ml DNase (Sigma-Aldrich, St. Louis, MO) at 37°C for 20 min. For the last 5 min, EDTA was added at 5 mM. Single-cell suspensions were prepared after RBC lysis. CD11c$^+$ cells were purified by MACS with anti-CD11c microbeads and used as splenic DCs. Enriched cells contained >90% CD11c$^+$ cells.

To prepare in vitro bone marrow-derived DCs (BMDCs), BM cells were prepared from femora and tibia and passed through nylon mesh. Then cells were cultured in RPMI 1640 medium supplemented with 10% FCS, 100 μM 2-ME, and 100 ng/ml human Flt3 ligand (Flt3L; PeproTech EC, London, U.K.). After 6–8 days, the cells were used as Flt3L-induced BMDCs (Flt3L-BMDCs) for additional experiments. Flt3L-BMDCs on days 6–8 contained 80–90% CD11c$^+$ cells, as described previously (14).

Flow cytometry

Splenic CD11c$^+$DCs or Flt3L-BMDCs were first incubated with biotinylated anti-CD11c and then with PE-conjugated anti-B220 and CyChrome-conjugated streptavidin. As indicated in Fig. 2, B220$^+$ and B220$^-$ cells were sorted using a FACSVantage (BD Bioscience, Mountain View, CA).

To evaluate surface expression levels of costimulatory molecules, cells were stained with biotinylated anti-CD40 and FITC-labeled anti-CD86, developed with PE-conjugated streptavidin, and analyzed on a FACSCalibur (BD Bioscience).

Measurement of cytokine production

Cells were seeded into 96-well plates at 2 × 10^6 cells/ml, or as otherwise indicated, in RPMI 1640 with 10% FCS and stimulated with various doses of synthesized oligodeoxynucleotides for 24 h. Culture supernatants were collected and analyzed for cytokine production. Cytokine concentrations in the supernatants were measured with ELISA. ELISA kits for mouse IFN-α were purchased from PBL Biomedical Laboratories (New Brunswick, NJ). ELISA kits for mouse TNF-α and IL-12 p40 were obtained from TECHNE Corp. (Minneapolis, MN).

Northern blot analysis

Total RNAs were isolated using Sepazol-RNA I (Nacalai Tesque, Kyoto, Japan), electrophoresed, and transferred to nylon membranes. Hybridization was performed with the indicated cDNA probes as described previously (11). cDNA probes specific for IFN-β, IL-12 p40, and IRF7 were obtained though the previously published subtractive screenings (15). The IFN-α probe is an *Eco*RI-*Hin*dIII fragment of the murine IFN-α4 and detects multiple IFN-α subtypes (16).

Results

Cytokine production of splenic DCs in response to CpG DNAs

We first evaluated CpG DNA-induced production of cytokines in splenic CD11c$^+$ DCs (Fig. 1*A*). D19 and ODN1668 were chosen as representatives of A/D-type and conventional CpG DNAs, respectively. Both increased the production of TNF-α and IL-12 p40 from splenic DCs in a dose-dependent manner, although D19 needed higher concentrations than ODN1668 to achieve comparable levels of cytokine production (Fig. 1).

We next measured IFN-α production of CpG DNA-stimulated splenic DCs. D19-induced IFN-α secretion was detected above a concentration of 0.1 μM and increased in a dose-dependent manner. ODN1668 could also induce IFN-α, but the production was only detected at concentrations of 0.01–0.3 μM and was abolished at higher concentrations. Furthermore, the maximal induction was much less than that of D19-stimulated DCs. Thus, ODN1668 and D19 have differential activities on mouse DCs in terms of IFN-α production.

In the presence of Flt3L, CD11c$^+$ cells, including IFN-α-producing cells, can be generated in vitro from BM cells (14). We next tested the responses of Flt3L-BMDCs to D19 and ODN1668.

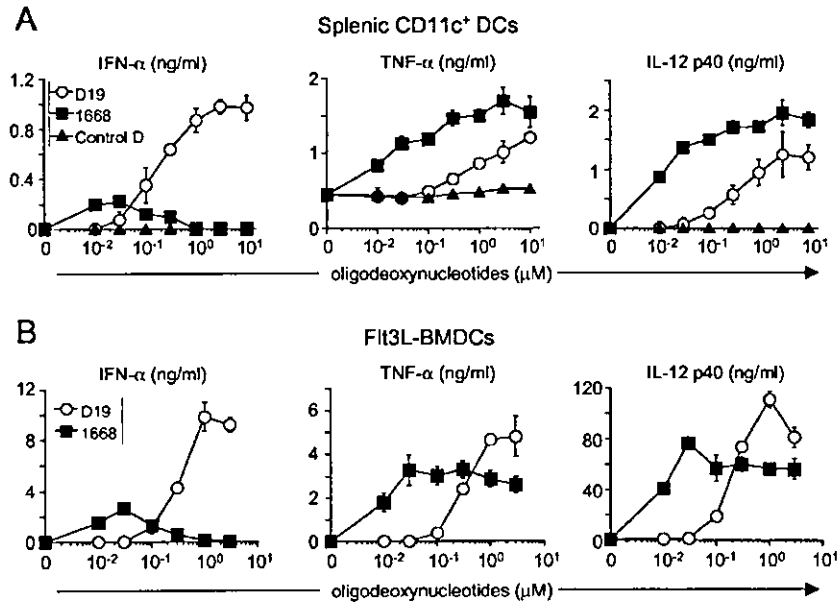

FIGURE 1. Cytokine production by splenic CD11c$^+$ cells (*A*) and Flt3L-BM DCs (*B*) in response to CpG DNAs. Splenic CD11c$^+$ cells were enriched by MACS and stimulated with the indicated concentrations of synthetic oligodeoxynucleotides for 24 h. Control D carries GpC instead of the CpG dinucleotide sequence of D19. Concentrations of IFN-α, TNF-α, and IL-12 p40 in the culture supernatants were measured by ELISA. Data are shown as the mean ± SD.

These DCs could also produce TNF-α and IL-12p40 in response to D19 or ODN1668. Similar to splenic DCs, Flt3L-BMDCs also responded better to ODN1668 than to D19. D19 could induce Flt3L-BMDCs to produce IFN-α in a dose-dependent manner, while ODN1668 induced small amounts of IFN-α only at 0.01–0.3 μM. Taken together, not only splenic CD11c$^+$, but also in vitro DCs, differentially responded to the two types of CpG DNAs in a similar manner.

B220$^+$ CD11c$^+$ cells are major IFN-α-producing cells in response to D19

DCs can be divided into subsets according to their surface molecule expression profiles (17). Among splenic DC subsets, B220$^+$CD11c^{dull} cells show a unique ability to produce IFN-α upon viral infection (18–21). To characterize the cell population involved in cytokine production from CpG DNA-stimulated splenic DCs, we purified B220$^+$CD11c^{dull} and B220$^-$CD11c^{high} cells by cell sorting and analyzed their responses to ODN1668 or D19 (Fig. 2*A*). In response to ODN1668, both B220$^+$CD11c^{dull} and B220$^-$CD11c^{high} cells produced IL-12 and enhanced their surface expression of CD40 and CD86. Neither population produced detectable levels of IFN-α in response to 3 μM ODN1668. In the case of D19 stimulation, both populations showed increased expression of costimulatory molecules. However, B220$^-$CD11c^{high} cells produced IL-12, but not IFN-α, whereas B220$^+$CD11c^{dull} cells produced IFN-α, but not IL-12.

Flt3L-BMDCs can also be divided into two subsets according to B220 expression (14). We next tested the responses of these subpopulations to CpG DNAs. The B220$^+$ and B220$^-$ cells in Flt3L-BMDCs responded to the two types of CpG DNAs in a manner similar to that of splenic B220$^+$CD11c^{dull} and B220$^-$CD11c^{high} cells, respectively (Fig. 2*B*). Thus, ODN1668 could activate both populations indistinguishably, whereas D19 showed differential cytokine-inducing ability in the two populations.

IFN-α production in response to D19 is dependent on TLR9 and MyD88

TLR9 or its cytoplasmic adapter, MyD88, is essential for conventional CpG DNA signaling (8, 22, 23). We next investigated whether the two types of CpG DNAs show any differences in their dependency on TLR9 or MyD88. Among splenocytes, CD11c$^+$ cells were mainly involved in IFN-α production in response to D19 (Fig. 3*A*). This IFN-α production was completely abolished in the absence of TLR9 or MyD88. Furthermore, whole and CD11c$^+$ splenocytes from TLR9$^{-/-}$ or MyD88$^{-/-}$ mice lacked both ODN1668- and D19-induced IL-12 production (Fig. 3*A*).

Next, we investigated the cytokine-producing ability of CpG DNA-stimulated Flt3L-BMDCs. IL-12 production in response to both types of CpG DNAs was abolished in Flt3L-BMDCs derived from both TLR9$^{-/-}$ and MyD88$^{-/-}$ mice (Fig. 3*B*). Furthermore, IFN-α production in response to D19 as well as that to 0.03 μM ODN1668 were completely abolished in the mutant Flt3L-BMDCs. Thus, the ability of both conventional and A/D-type CpG DNAs to induce cytokine production from in vivo and in vitro DCs was dependent on TLR9 and MyD88.

DNA-PKcs is not essential for responses to CpG DNA

It has been reported that DNA-PKcs is necessary for cytokine production in response to CpG DNAs, because DNA-PKcs$^{-/-}$ cells lacked the response (24). We next examined cytokine production of DNA-PKcs$^{-/-}$ cells in response to CpG DNAs. DNA-PKcs$^{-/-}$ mice lack mature B and T cell population due to defective DNA recombination (12, 25). Therefore, CD11c$^+$ cells were isolated by MACS from wild-type and mutant splenocytes. Splenic CD11c$^+$ cells were stimulated with D19 or ODN1668 for 24 h and analyzed for their cytokine production (Fig. 4*A*). DNA-PKcs$^{-/-}$ CD11c$^+$ cells retained the ability to produce IFN-α and IL-12 in response to CpG DNAs.

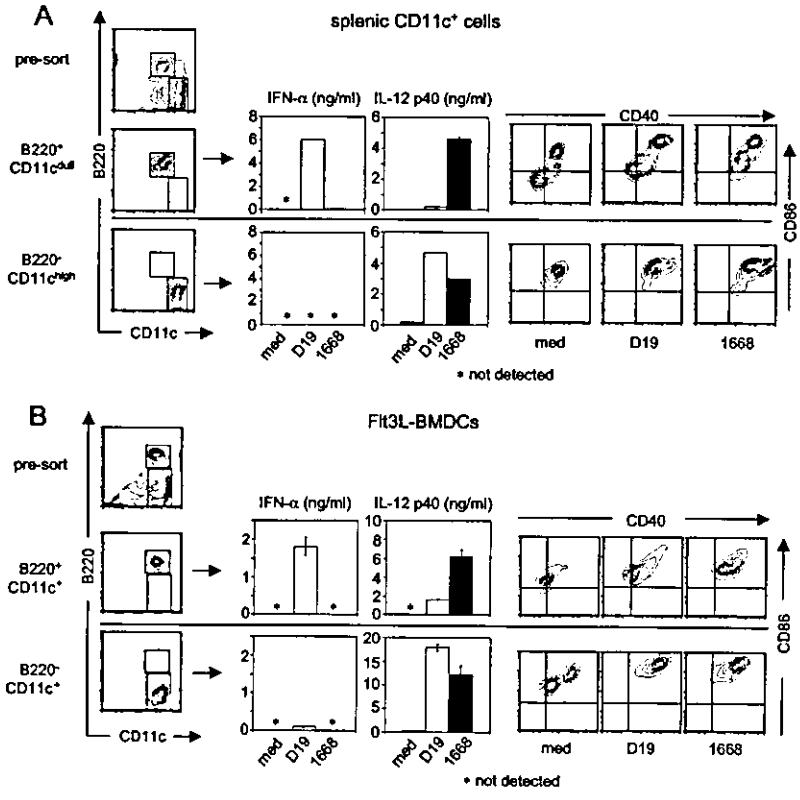

FIGURE 2. B220$^+$CD11c$^+$ and B220$^-$CD11c$^+$ cells differentially respond to two types of CpG DNAs. Splenic B220$^+$CD11c^{dull} and B220$^-$CD11c^{high} cells (*A*) were purified by FACS. Sorted cells were cultured at 4 × 10^4 cells/well with or without 3 μM CpG DNAs for 24 h. Concentrations of IFN-α or IL-12 p40 were measured by ELISA and are shown as the mean ± SD. Surface expression of costimulatory molecules was analyzed by flow cytometry. Flt3L-BMDCs (*B*) were also sorted by B220 expression and analyzed similarly to splenic DCs. Reanalysis of sorted cells verified that >95% cells exhibited the expected FACS profiles.

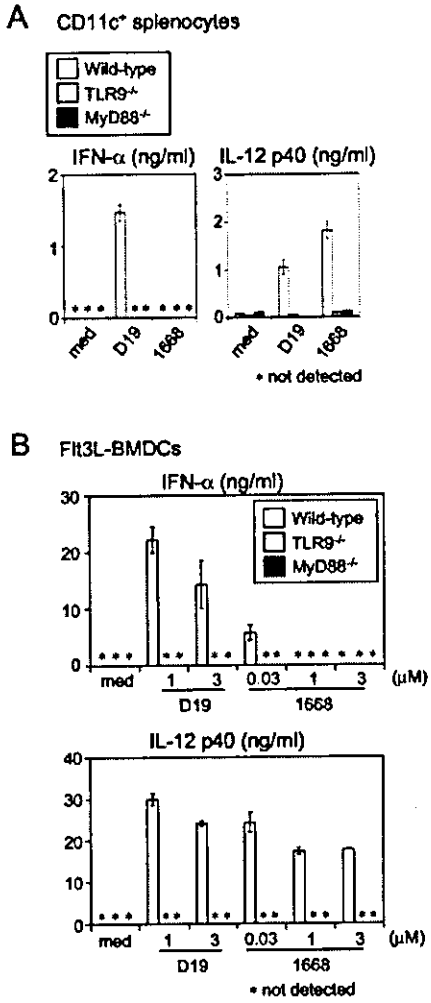

FIGURE 3. TLR9$^{-/-}$ or MyD88$^{-/-}$ cells lack any cytokine production in response to either type of CpG DNA. Splenic CD11c$^+$ DCs (*A*) and Flt3L-BMDCs (*B*) were prepared from wild-type, TLR9$^{-/-}$, or MyD88$^{-/-}$ mice. Cells were stimulated with the indicated concentrations of D19 or ODN1668 for 24 h. Concentrations of IFN-α and IL-12 p40 were measured by ELISA. Data are shown as the mean ± SD of one representative experiment.

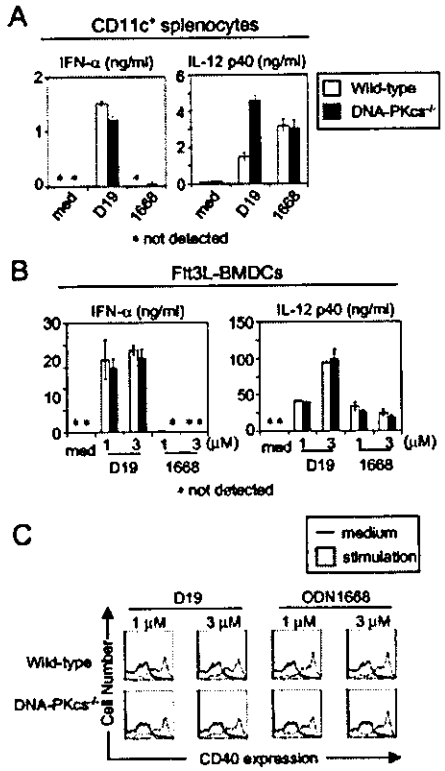

FIGURE 4. DNA-PKcs$^{-/-}$ cells normally respond to CpG DNAs. Splenic CD11c$^+$ DCs (*A*) and Flt3L-BMDCs (*B*) from wild-type or DNA-PKcs$^{-/-}$ mice were stimulated with 3 μM D19 or ODN1668 (1668) for 24 h. Concentrations of IFN-α and IL-12 p40 in the culture supernatants were measured by ELISA. Data are shown as the mean ± SD. Surface expression of CD40 on Flt3L-BMDCs was analyzed by flow cytometry (*C*). Similar results were obtained from three independent experiments.

We also analyzed the effects of both CpG DNAs on wild-type and DNA-PKcs$^{-/-}$ Flt3L-BMDCs. FACS analysis revealed that the population ratio of B220$^+$CD11c$^+$ and B220$^-$CD11c$^+$ cells in Flt3L-BMDCs from DNA-PKcs$^{-/-}$ mice was comparable to that from wild-type mice (data not shown). DNA-PKcs$^{-/-}$ Flt3L-BMDCs augmented IL-12 production and surface expression of CD40 and CD86 in response to ODN1668 (Fig. 4, *B* and *C*, and data not shown). These responses were also observed in D19-stimulated DNA-PKcs$^{-/-}$ Flt3L-BMDCs. Furthermore, the mutant BMDCs produced IFN-α in response to D19 (Fig. 4*B*). Thus, these results clearly indicated that DNA-PKcs are dispensable for all immunostimulatory effects of both types of CpG DNAs.

Northern blot analysis of CpG DNA-stimulated DCs

IRF7 expression is induced by type I IFNs or viral infection and involved in type I IFN production (16, 26, 27). Therefore, we examined whether the IRF7 mRNA is differentially induced by the two types of CpG DNAs. As shown in Fig. 5*A*, IRF7 mRNA induction was observed in D19-stimulated Flt3L-DCs. ODN1668 also up-regulated IRF7 mRNA expression at both low and high concentrations with similar kinetics and levels as D19, although induction of IFN-α and IFN-β mRNA was abolished in DCs stimulated with high concentrations of ODN1668.

It has been reported that in viral infections, IRF7 mRNA induction is dependent on IFN-α/β (27). Therefore, we analyzed gene expression of CpG DNA-stimulated IFN-α/βR-deficient (IFN-α/βR$^{-/-}$) DCs. IL-12p40 mRNA induction by both CpG DNAs was retained in IFN-α/βR$^{-/-}$ DCs (Fig. 5*B*). However, IFN-α/β mRNA up-regulation by D19 was abolished in the absence of IFN-α/βR (Fig. 5*B*), indicating the critical involvement of type I IFN signaling in type I IFN production induced by D19. Furthermore, IRF7 mRNA induction by D19 as well as by ODN1668 was abolished in the absence of IFN-α/βR. This suggests that type I IFN signaling is essential for IRF7 mRNA induction even in ODN1668-stimulated DCs. These data, however, indicate that the loss of IFN-α mRNA induction at higher doses of ODN1668 may not be due to a decrease in IRF7 induction.

Discussion

In this study we analyzed cellular and molecular basis for the actions of two types of CpG DNAs. Conventional CpG DNAs can activate murine DCs to produce IL-12 and enhance the surface expression of costimulatory molecules. A/D-type CpG DNAs can also activate murine DCs in a similar manner as conventional CpG DNAs and, moreover, can induce IFN-α production from CD11c$^+$ cells. Splenic CD11c$^+$ cells can be divided into two populations, B220$^+$CD11c^{dull} and B220$^-$CD11c^{high} cells. The former cells were identified as IFN-α-producing cells during viral infection